

Synthesis Design

Pyridyl-Functionalised 3*H*-1,2,3,4-Triazaphospholes: Synthesis, Coordination Chemistry and Photophysical Properties of Low-Coordinate Phosphorus CompoundsJulian A. W. Sklorz,^[a] Santina Hoof,^[a] Nadine Rades,^[a] Nicolas De Rycke,^[b] László Könczöl,^[c] Dénes Szieberth,^[c] Manuela Weber,^[a] Jelena Wiecko,^[a] László Nyulászi,^{*[c]} Muriel Hissler,^{*[b]} and Christian Müller^{*[a]}

Dedicated to Professor Manfred Scheer on the occasion of his 60th birthday

Abstract: Novel conjugated, pyridyl-functionalised triazaphospholes with either *t*Bu or SiMe₃ substituents at the 5-position of the N₃PC heterocycle have been prepared by a [3+2] cycloaddition reaction and compared with structurally related, triazole-based systems. Photoexcitation of the 2-pyridyl-substituted triazaphosphole gives rise to a significant fluorescence emission with a quantum yield of up to 12%. In contrast, the all-nitrogen triazole analogue shows no emission at all. DFT calculations indicate that the 2-pyridyl substituted systems have a more rigid and planar structure than their 3- and 4-pyridyl isomers. Time-dependent (TD) DFT calculations show that only the 2-pyridyl-substituted tri-

azaphosphole exhibits similar planar geometry, with matching conformational arrangements in the lowest energy excited state and the ground state; this helps to explain the enhanced emission intensity. The chelating P,N-hybrid ligand forms a Re^I complex of the type [(N[^]N)Re(CO)₃Br] through the coordination of nitrogen atom N² to the metal centre rather than through the phosphorus donor. Both structural and spectroscopic data indicate substantial π-accepting character of the triazaphosphole, which is again in contrast to that of the all-nitrogen-containing triazoles. The synthesis and photophysical properties of a new class of phosphorus-containing extended π systems are described.

Introduction

Low-coordinate phosphorus compounds have recently regained noticeable interest because the very peculiar electronic and steric properties of such λ³,σ²-species differ significantly from classical trivalent λ³,σ³-phosphanes. Their special characteristics can lead to interesting properties in more applied research fields, such as homogeneous catalysis or molecular materials science.^[1] For example, pyridyl-functionalised phosphinines (phosphabenzenes) of type **A** (Figure 1) have been used for the development of coordination compounds that present

interesting reactivities and structural motifs.^[2] Another class of low-coordinate phosphorus heterocycles are 3*H*-1,2,3,4-triazaphospholes. These compounds have a conjugated π system with a high degree of aromaticity and possess a rather high π density at the phosphorus atom due to significant N=C=P↔N⁺=C-P⁻ conjugation.^[3,4] We have recently demonstrated that methylene-bridged, pyridyl-functionalised triazaphospholes of type **B** (Figure 1) can be used to develop transition-metal complexes with different properties from the analogous triazole-based systems.^[5] However, it should be noted that the pyridine and five-membered ring are not in direct conjugation in compound **B**.

Coordination compounds containing chelating N[^]N ligands, such as 2,2'-bipyridine (bipy) or phenanthroline (phen; **C**, Figure 2) have been exploited, to a large extent, as functional components in electronic and luminescent materials, as well as

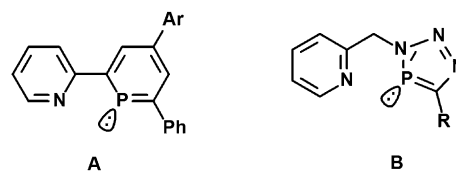


Figure 1. 2-(2'-Pyridyl)-4,6-arylphenylphosphinine **A** and 2-(((5-R)-3*H*-1,2,3,4-triazaphosphole-3-yl)methyl)pyridine **B**.

[a] J. A. W. Sklorz, S. Hoof, N. Rades, M. Weber, Dr. J. Wiecko, Prof. Dr. C. Müller
Institut für Chemie und Biochemie, Anorganische Chemie
Freie Universität Berlin, Fabeckstr. 34/36, 14195 Berlin (Germany)
E-mail: c.mueller@fu-berlin.de

[b] Dr. N. De Rycke, Prof. Dr. M. Hissler
Institut des Sciences Chimiques de Rennes
UMR 6226 CNRS - Université de Rennes 1, Campus de Beaulieu
35042 Rennes Cedex (France)
E-mail: muriel.hissler@univ-rennes1.fr

[c] L. Könczöl, Dr. D. Szieberth, Prof. Dr. L. Nyulászi
Budapest University of Technology and Economics
Department of Inorganic and Analytical Chemistry
Szt. Gellért tér 4, 1521 Budapest (Hungary)
E-mail: nyulaszi@mail.bme.hu

Supporting information for this article is available on the WWW under
<http://dx.doi.org/10.1002/chem.201500988>.

photocatalysts for the reduction of CO₂. Consequently, it could be interesting to develop novel ligand systems with the pyridine and the triazaphosphole moieties in direct conjugation.^[6] Those compounds could be derived from pyridyl-functionalised triazoles of type **D** (Figure 2), which have recently emerged as readily modified bipy and phen surrogates as well. Triazoles are generally accessible in a facile manner by a Cu^I-catalysed 1,3-cycloaddition reaction, starting from 2-ethynylpyridine and organic azides (R–N₃).^[7] In this respect, it is important to note that the related reaction towards N-heterocycle-substituted 1,2,3-triazoles of type **E** (inverse click product relative to **D**), starting from 2-azidopyridine, is not straightforward because this azide exists in equilibrium between a closed form (tetrazole **F**) and the open form (azide **G**; Figure 2). Indeed, it has been shown that pyridotetrazole **F** is inert towards click reactions under standard conditions because the equilibrium for this particular compound is shifted far to the left (Figure 2).^[8] However, few examples have been reported in the literature on successful click reactions of alkynes with pyridotetrazoles at *T* = 120 °C, and the coordination chemistry of such inverse 2-pyridyl-triazoles has been investigated to some extent.^[9]

This inherent drawback seems to be particularly problematic for the synthesis of pyridyl-functionalised triazaphospholes because one has to start from pyridotetrazole as an azide surrogate, since pyridine-derived phosphalkynes are not available. Nevertheless, we envisaged access to a family of novel pyridyl-functionalised, conjugated triazaphospholes of type **H**, with the nitrogen atom in either the 2-, 3- or 4-positions of the pyridyl-moiety (Figure 3).

The chelating version of **H** (2-pyridyl-**H**) should not only be interesting from a coordination chemistry point of view, but it also closely resembles structurally donor-functionalised phosph-

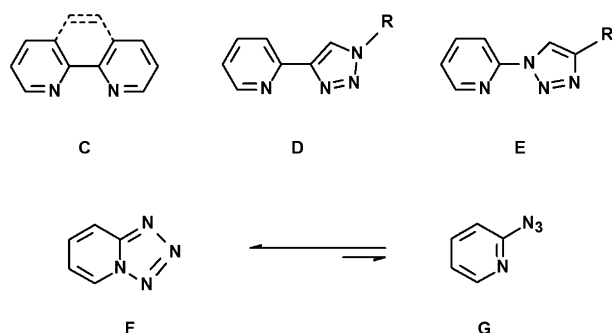


Figure 2. Common chelating N^N ligands and pyridotetrazole-2-azidopyridine equilibrium.

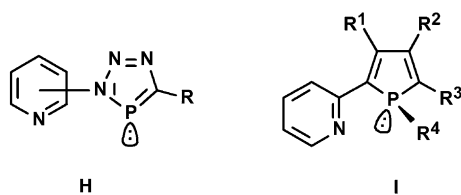


Figure 3. Comparison between pyridyl-functionalised triazaphospholes (**H**) and phospholes (**I**).

holes, such as **I** (Figure 3). These five-membered phosphorus heterocycles, as well as their corresponding transition-metal complexes, have gained tremendous interest as π -conjugated components in organic light-emitting diodes (OLEDs).^[10] It thus appeared surprising to us that no studies on the photophysical properties of 3*H*-1,2,3,4-triazaphospholes had appeared in the literature to date. It should, however, be mentioned that 2-pyridylphospholes contain an exocyclic P substituent and are less aromatic than triazaphospholes, which should certainly have an impact on the respective properties.

We report herein on a detailed investigation into the synthesis of pyridyl-substituted, conjugated 3*H*-1,2,3,4-triazaphosphole derivatives **1 a/b–3 a**, as well as on the coordination chemistry of chelates **1 a/b** towards Re^I. Moreover, the photophysical properties of these compounds are evaluated by measuring the excitation and emission spectra and the results are interpreted by means of DFT calculations. Selected compounds are compared with the reference compounds **4 a/b** and **5 a/b** to gain information on the influence of the heteroatoms and on the importance of conjugation between heterocycles with respect to their luminescence properties. As such, the triazaphosphole is attached directly to a phenyl moiety in **4 a/b**, which allows π conjugation, but lacks the nitrogen atom in the six-membered ring. In **5 a/b**, π conjugation with the phenyl moiety is interrupted (Figure 4). Considering the diagonal relationship of the phosphorus carbon, triazaphospholes are also compared with structurally related triazoles.^[11]

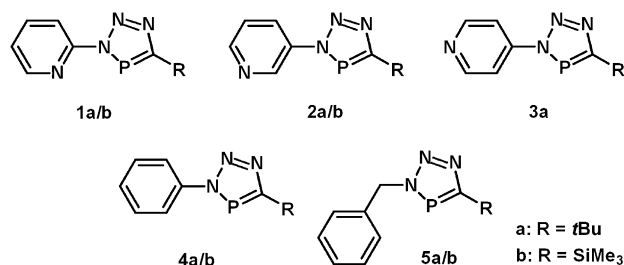


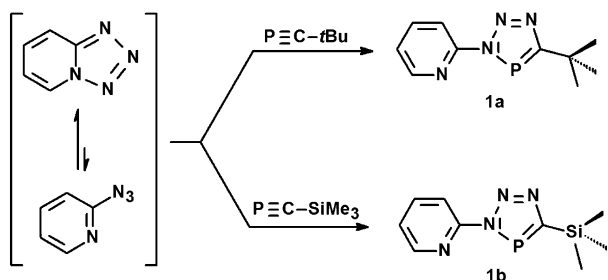
Figure 4. Pyridyl-functionalised triazaphospholes and reference compounds.

Results and Discussion

Synthesis and characterisation

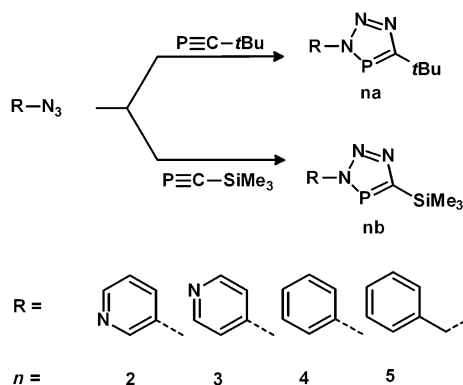
For the preparation of compound **1 a**, pyridotetrazole **F** (Figure 2) was synthesised according to a literature procedure.^[9a] We first attempted the reaction of **F** with *tert*-butylphosphalkyne (P≡C–*t*Bu) at *T* = 125 °C in toluene. This temperature was chosen with the intention of shifting the equilibrium **F/G** sufficiently to the azide form (Scheme 1).^[12] The ³¹P{¹H} NMR spectrum of the dark red–brown reaction mixture revealed the presence of one main product at δ = +167.5 ppm, but several unidentified by-products appeared, which could not be separated from the main product. Subsequently, the [3+2] cycloaddition reaction was carried out at lower temperature (*T* = 60–80 °C) and the conversion was again followed by means of

$^{31}\text{P}\{^1\text{H}\}$ NMR spectroscopy. Much to our surprise, the reaction was selective and ran to completion after one week. The novel triazaphosphole **1a** was obtained in 98% yield (determined spectroscopically) as a pale-yellow solid after removal of the solvent (Scheme 1). Similarly, the SiMe_3 -substituted triazaphosphole **1b** was formed within 1 h through the reaction of the pyridotetrazole and $\text{P}\equiv\text{C}-\text{SiMe}_3$ in toluene at $T=65^\circ\text{C}$; the product was isolated as an orange oil.^[13] The SiMe_3 group had a great influence on the chemical shift of the product: the resonance of **1b** was observed at $\delta=+211.6$ ppm in the $^{31}\text{P}\{^1\text{H}\}$ NMR spectrum.



Scheme 1. Synthesis of **1a/b** starting from pyridotetrazole.

The pyridyl-functionalised triazaphospholes **2a/b**, **3a**, **4a/b** and **5a/b**^[14] could be prepared as well, starting from the corresponding azides. The [3+2] cycloaddition reaction with both phosphalkynes proceeded smoothly at room temperature in toluene within several minutes in each case (Scheme 2). Compound **3b** ($\text{R}=\text{SiMe}_3$) could not be obtained in a pure form. It should be noted here that the Me_3Si -substituted triazaphospholes seemed to be light sensitive.



Scheme 2. Synthesis of pyridyl-functionalised triazaphospholes and reference compounds.

Crystals of **1a**, **2a**, **3a**, **4a**, **5a** and **5b** suitable for a crystallographic characterisation were obtained from a saturated solution in pentane at $T=-20^\circ\text{C}$. Although the two ring systems are coplanar in **1a** (Figure 5) and **3a** (Figure S1 in the Supporting Information), they are considerably twisted in **2a** and **4a**, with dihedral angles of 38.7° (Figure 6) and 46.5° , respectively

(Figure S2 in the Supporting Information). The molecular structures of **5a** and **5b** are very similar concerning the location of the benzyl group with respect to the planar triazaphosphole heterocycle (Figures S3 and S4 in the Supporting Information). Interestingly, although known for many years, only a few 3*H*-1,2,3,4-triazaphospholes have so far been characterised crystallographically by Jones et al.^[15] All available structural parameters indicate significant conjugation within the heterocycles. In case of **1a**, the $\text{P}(1)-\text{C}(1)$ distance (1.7133(19) Å) is slightly shorter than the $\text{P}-\text{C}$ bond lengths in 2,4,6-triarylphosphinines (≈ 1.75 Å). It thus lies between the values of a localised $\text{P}=\text{C}$

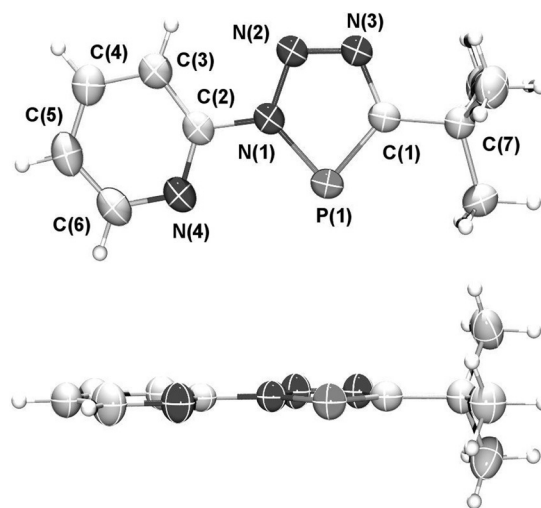


Figure 5. Molecular structure of a crystal of **1a**. Displacement ellipsoids are shown at the 50% probability level. Selected bond lengths [Å] and angles [°]: $\text{P}(1)-\text{C}(1)$: 1.7133(19), $\text{P}(1)-\text{N}(1)$: 1.7012(16), $\text{C}(1)-\text{N}(3)$: 1.368(2), $\text{N}(3)-\text{N}(2)$: 1.300(2), $\text{N}(2)-\text{N}(1)$: 1.353(2), $\text{N}(1)-\text{C}(2)$: 1.436(2), $\text{C}(2)-\text{N}(4)$: 1.321(2), $\text{C}(2)-\text{C}(3)$: 1.383(3), $\text{N}(4)-\text{C}(6)$: 1.344(3), $\text{C}(1)-\text{C}(7)$: 1.519(3); $\text{C}(1)-\text{P}(1)-\text{N}(1)$: 85.77(8), $\text{N}(1)-\text{N}(2)-\text{N}(3)$: 110.54(15), $\text{N}(2)-\text{N}(1)-\text{C}(2)-\text{C}(3)$: 0.0.

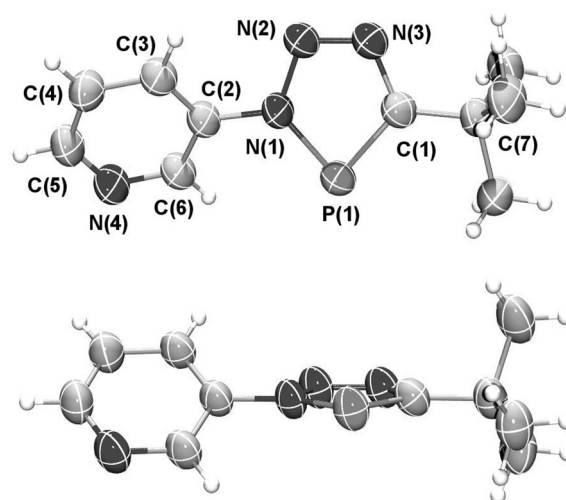


Figure 6. Molecular structure of a crystal of **2a**. Displacement ellipsoids are shown at the 50% probability level. Selected bond lengths [Å] and angles [°]: $\text{P}(1)-\text{C}(1)$: 1.717(6), $\text{P}(1)-\text{N}(1)$: 1.696(4), $\text{C}(1)-\text{N}(3)$: 1.370(8), $\text{N}(3)-\text{N}(2)$: 1.320(7), $\text{N}(2)-\text{N}(1)$: 1.358(6), $\text{N}(1)-\text{C}(2)$: 1.444(7), $\text{C}(2)-\text{C}(3)$: 1.376(8), $\text{C}(2)-\text{C}(6)$: 1.388(7), $\text{N}(4)-\text{C}(6)$: 1.341(8), $\text{C}(1)-\text{C}(7)$: 1.513(8); $\text{C}(1)-\text{P}(1)-\text{N}(1)$: 86.6(3), $\text{N}(2)-\text{N}(1)-\text{C}(2)-\text{C}(3)$: $-38.7(8)$.

double bond ((diphenylmethylene)(mesityl)phosphine; MesP=CPh₂: 1.692 Å) and a P–C single bond (PPh₃: 1.83 Å).^[16] The N–P–C angle is, at 85.77(8)°, almost 90° and differs significantly from the C–P–C angle in the aromatic six-membered phosphorus heterocycles (≈ 100°).^[17]

The near 90° bond angle, which is characteristic for these phosphorus compounds, can apparently more easily be achieved in a planar pentagon (ideally 107°) than in a hexagon (ideally 120°). This can be explained by the fact that the lighter sp²-hybridised ring atoms strive for the trigonal planar arrangement. A similar effect contributes to the planarisation of the σ^3 -P atom in polyphosphaphospholes.^[18] As suggested by Nyulászi et al., all of these observations are in agreement with significant aromaticity within 1,2,3,4-triazaphospholes.^[3]

Because the co-planarity of the two aromatic rings is clearly related to π conjugation and is supposed to affect the optical properties (see below), the relevant structural parameters in the triazaphosphole rings of **1 a–5 a/b** are compared in Table 1.

	N1–C2	N2–N1	N3–N2	C1–N3	P1–C1	P1–N1
1 a	1.436	1.353	1.300	1.368	1.713	1.701
2 a	1.444	1.358	1.320	1.370	1.717	1.696
3 a	1.435	1.352	1.303	1.353	1.704	1.694
4 a	1.436	1.350	1.309	1.351	1.711	1.689
5 a	1.484	1.340	1.314	1.351	1.712	1.683
5 b	1.485	1.345	1.314	1.368	1.709	1.679

It is noteworthy that the structural parameters for the conjugated rings in **1 a–4 a** remain virtually unchanged, considering experimental error, irrespective of whether the two rings are coplanar or not. Likewise, the interatomic triazaphosphole ring distances in non-conjugated **5 a** are similar to those in **1 a–4 a**. However, in this case, both formally single bonded P(1)–N(1) and N(2)–N(1) distances are slightly shorter, which indicates some enhancement of delocalisation of the nitrogen lone pair within the five-membered ring. Accordingly, the N1–C2 distance in **5 a** is significantly longer than those in conjugated compounds **1 a–4 a**. Here, the distance between the two rings is similar, within experimental error, for both planar and non-planar systems. By taking these observations into account, it can be concluded that some conjugation remains effective between the five- and six-membered heterocycles, even in the partially twisted forms.

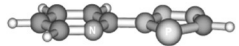
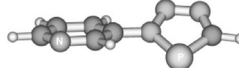
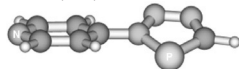
To investigate the extent of co-planarity in **1 a–4 a** in more detail, quantum chemical calculations were carried out. The structures of the H-substituted

triazaphospholes **I** (2-py), **II** (3-py) and **III** (4-py) were calculated with different DFT functionals and basis sets to probe the reliability of our results (Table 2).

Clearly, the most stable structure is **I**, with the pyridyl nitrogen and phosphorus atoms in the *cis* position. This is in agreement with results obtained from the crystallographic characterisation of **1 a** (Figure 5). The energetic preference is approximately 5 kcal mol^{−1} with respect to all other isomeric structures at each investigated level of theory. Since this relative stability remains unchanged when functionals with a dispersion correction were used, it seems that this energetic preference is not a consequence of steric repulsion. Also, no pnictogen interactions between phosphorus and pyridyl nitrogen atoms are present. In fact, neither a bond critical point was located between the phosphorus and nitrogen atoms, nor was any stabilising interaction found in the second-order perturbation analysis carried out on the basis of natural bond orbitals (NBOs).^[19] By considering the nearly uniform destabilisation of the other structures, it seems that a N–P repulsive interaction is simply smaller than N...N or (C)H...N/P non-bonded repulsive interactions. By calculating planar *trans-I* with P and N atoms in the *trans* position with respect to one another, a saddle point with an additional destabilisation of 1.6 kcal mol^{−1} was obtained, which was in agreement with the expected repulsive N...N interaction.

Although the planarity of **I** is in agreement with structural analysis of **1 a**, the optimised structure of **III** is non-planar, which is in contrast with the planarity of **3 a** in the crystal (Figure S1 in the Supporting Information). Thus, we further determined the rotational barrier around the interconnecting N(1) and C(pyridyl) atoms of **1 a**, **2 a** and **3 a** and the results are depicted in Figure 7. The rotational barrier is largest for 2-pyridyl-substituted triazaphosphole **1 a**. In this case, the minimum energy is related to a planar structure, in which phosphorus and nitrogen atoms of **1 a** in the *cis* position (dihedral angle is 0°) is the most stable conformation. We found an additional non-planar minimum near to the *trans* arrangement of the phosphorus and nitrogen atoms, which was less stable by about 5 kcal mol^{−1}. In the case of **2 a** (3-pyridyl), the energy difference between the twisted minimum structure and the planar (transition) structure is 0.4 kcal mol^{−1}, whereas it is even

Table 2. Comparison of the relative energies (E_{rel}) of the minimised structures of triazaphospholes with different functionals and basis sets.

	ω B97xD/aug-cc-pVTZ	E_{rel} [kcal mol ^{−1}] ω B97xD/6-31 + G*	B3LYP/aug-cc-pVTZ
 <i>cis</i> -2-pyridyltriazaphosphole (I)	0.0	0.0	0.0
 <i>cis</i> -3-pyridyltriazaphosphole (II)	5.5	5.5	5.6
 4-pyridyltriazaphosphole (III)	4.9	4.9	5.0

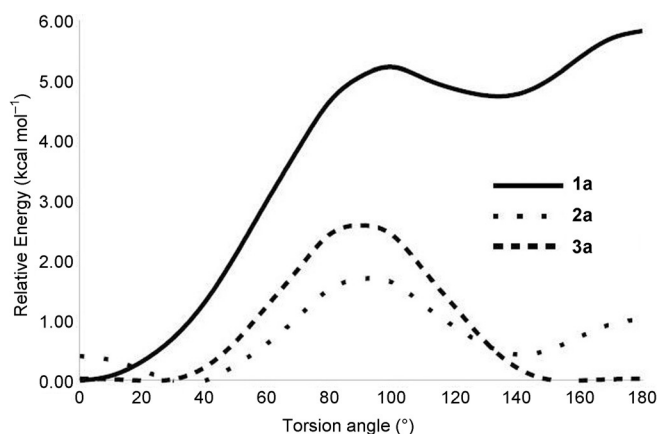


Figure 7. ω B97xD/aug-cc-pVDZ rotational barriers for the different pyridyl-triazaphospholes (**1a–3a**). The reference energy is the lowest energy minimum for each compound, which shows the difference in the barriers; however, it should be noted that **1a** is more stable than **2a** or **3a** by 5 kcal mol⁻¹.

less than 0.1 kcal mol⁻¹ between 0 and 30° for **3a** (4-pyridyl). The planar structure is a first-order saddle point in both cases. The contrast between the calculated non-planar structure of **3a** and the observed planarity in X-ray crystal-structure analysis is understandable in light of the very small energy difference, when considering in particular that the calculations refer to the gas phase.

To understand the preference of a coplanar arrangement of the two heterocycles in the crystalline phase of **3a**, which is in contrast to the calculations, it is also noteworthy that **3a** shows interesting packing of the molecules in the crystal lattice (Figure 8). The two closest molecules are stacked in such a way that the phosphorus atoms lie above or below the respective pyridyl moiety and vice versa (Figure 8, upper left and lower right). The distance between the phosphorus atom of one triazaphosphole and the centroid of the pyridyl moiety of the second triazaphosphole is in the range of 3.58 Å. It should be noted here that this type of stacking is not observed in the crystal lattice of compound **1a**, despite the fact that the two rings are coplanar (Figure 8).

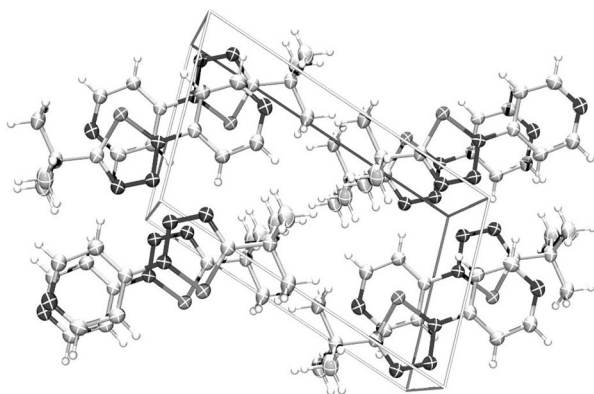
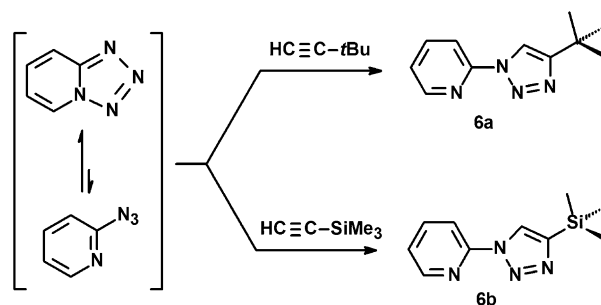


Figure 8. Packing in a crystal of **3a**. View along the *b* axis.

We also computed the dimeric structure of **3a** at the ω B97xD/6-311+G** level to investigate further the effect of this interaction. Although the two rings within one molecule did not remain fully planar, a significant 14 kcal mol⁻¹ (basis set superposition error (BSSE)-corrected ω B97xD/6-311+G**) interaction energy was obtained, which indicated that intermolecular interactions played a significant role in the crystalline phase. Atoms in molecules (AIM) analysis of the electron density did not reveal any bond critical points between the phosphorus atom and the six-membered ring of the neighbouring molecule.^[20]

To compare triazaphospholes **1a** and **1b**, in particular, with the corresponding phosphorus-lacking triazoles, which had otherwise identical substitution patterns, we also carried out the click reaction of pyridotriazole with either HC≡C-*t*Bu or HC≡C-SiMe₃ at *T* = 140 °C in toluene in the presence of CuOTf·C₆H₆ (Tf = triflyl) as the Cu catalyst, according to a modified literature procedure.^[9g] The pyridyl-functionalised triazoles **6a** and **6b** could be obtained straightforwardly in good yields as colourless, pure solids after removal of the solvent (Scheme 3).



Scheme 3. Synthesis of pyridyl-functionalised triazoles **6a/b** from 2-azidopyridine.

We were able to obtain crystals of **6a** that were suitable for XRD. The molecular structure of the 2-pyridyl-functionalised triazole is depicted in Figure 9.

Similar to the structurally related triazaphosphole, a *cis* alignment of the pyridyl nitrogen atom and C(2)–H group can be observed. This arrangement appears to be necessary to minimise non-bonded repulsive N...N and (C)H...N interactions. Moreover, the two nitrogen heterocycles are only slightly twisted with a dihedral angle of –19.42(17)°. The inter-ring distance of N(1)–C(3) (1.4273(16) Å) is only slightly shorter than that in triazaphosphole **1a** (1.436(2) Å), which again indicates significant conjugation between the five- and six-membered nitrogen heterocycles.

According to our calculations, the ω B97xD/aug-cc-pVTZ rotational surface of triazole **6a** is similar to that of triazaphosphole **1a**. The most stable minimum is a planar structure with a *cis* arrangement of the N(4)C(3)N(1)N(2) units. The rotational barrier is 6 kcal mol⁻¹, and a second non-planar minimum also exists close to the highest energy point of the rotational potential energy surface.

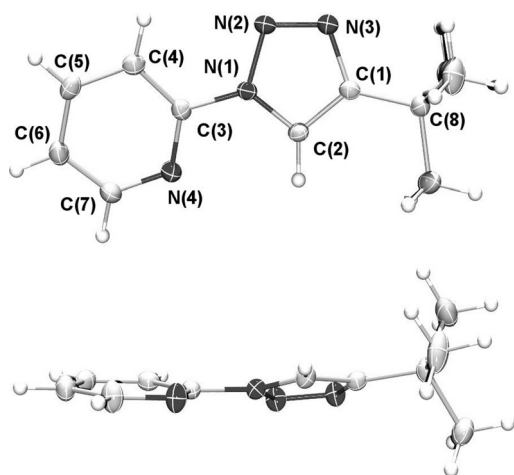


Figure 9. Molecular structure of a crystal of **6a**. Displacement ellipsoids are shown at the 50% probability level. Selected bond lengths [Å] and angles [°]: C(2)–C(1): 1.3639(17), C(1)–N(3): 1.3704(16), N(3)–N(2): 1.3136(15), N(2)–N(1): 1.3537(15), N(1)–C(2): 1.3541(16), N(1)–C(3): 1.4273(16), C(3)–N(4): 1.3281(16), C(3)–C(4): 1.3867(17), C(4)–C(5): 1.3836(18), C(5)–C(6): 1.3875(19), C(6)–C(7): 1.3817(19); C(1)–C(2)–N(1): 105.02(11), N(1)–N(2)–N(3): 106.71(10), N(2)–N(1)–C(3)–C(4): –19.42(17).

Coordination chemistry

We recently demonstrated that methylene-bridged triazaphospholes of type **B** (Figure 1) and the corresponding phosphorus-lacking triazoles underwent a facile reaction with $\text{Re}(\text{CO})_5\text{Br}$ to form complexes $[(\text{N}^{\wedge}\text{N})\text{Re}(\text{CO})_3\text{Br}]$.^[5] We therefore also decided to explore the coordination chemistry of **1a** and **6a** towards Re^I because those bidentate ligands were expected to coordinate in a chelating manner to a transition-metal centre, in contrast to compounds **2–4**. At the same time, the $[\text{Re}(\text{CO})_3\text{Br}]$ metal fragment offers the possibility of investigating the electronic properties of the ligands by means of IR spectroscopy of the resulting coordination compounds. We first paid attention to the coordination chemistry of the triazaphosphole, which could coordinate in either a $\text{P}^{\wedge}\text{N}$ (**J**) or an $\text{N}^{\wedge}\text{N}$ (**K**) fashion (Figure 10). Compound **1a** was thus reacted with an equimolar amount of $[\text{Re}(\text{CO})_3\text{Br}]$ in dichloromethane at $T=80^\circ\text{C}$ in a sealed NMR tube and the reaction was monitored by means of $^{31}\text{P}\{^1\text{H}\}$ NMR spectroscopy. After 8 h the conversion was complete and the reaction product showed a resonance in the $^{31}\text{P}\{^1\text{H}\}$ NMR spectrum at $\delta = +191.3$ ppm. From the chemical shift difference of $\Delta\delta = 23.8$ ppm it is, however, not conclusive whether the triazaphosphole moiety coordinates through the phosphorus or nitrogen lone pairs to the metal centre because σ -coordinated phosphinines show a similar chemical shift difference upon coordination to a metal centre (Figure 10).^[21]

Crystals of **7a**, suitable for X-ray crystal-structure analysis, were obtained from cooling a hot saturated solution of the compound in dichloromethane slowly to $T=-21^\circ\text{C}$. Compound **7a** crystallises in the space group $P\bar{1}$ and the molecular structure of the crystal, along with selected bond lengths and angles, is depicted in Figure 11; this shows the expected facial geometry of the $[\text{L}_2\text{Re}(\text{CO})_3\text{Br}]$ complex.

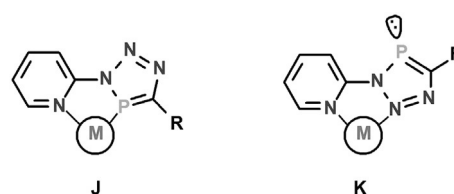


Figure 10. Possible coordination modes of **1a/b**.

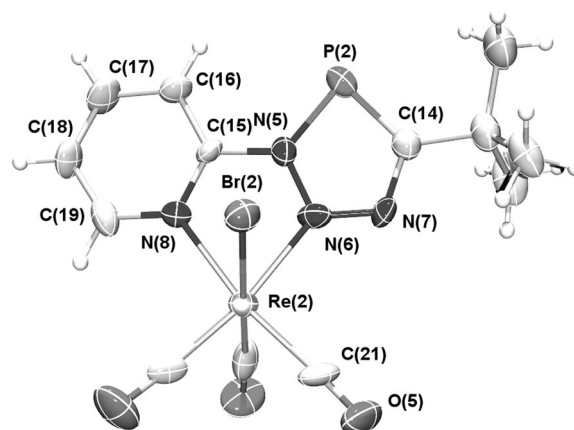


Figure 11. Molecular structure of a crystal of **7a**. Displacement ellipsoids are shown at the 50% probability level. Only one independent molecule is shown and the non-coordinated CH_2Cl_2 solvent molecules are omitted for clarity. Selected bond lengths [Å] and angles [°]: P(2)–C(14): 1.706(11), P(2)–N(5): 1.714(8), N(5)–N(6): 1.349(12), N(6)–N(7): 1.302(13), N(7)–C(14): 1.336(13), N(5)–C(15): 1.413(12), N(8)–Re(2): 2.179(11), N(6)–Re(2): 2.147(9); N(5)–P(2)–C(14): 85.4(5), N(8)–Re(2)–N(6): 73.6(4).

From crystallographic characterisation, it is clear that the chelating ligand **1a** coordinates to the Re^I centre through the nitrogen atom N(6) of the triazaphosphole moiety, rather than through the phosphorus atom. Interestingly, the coordination of the least nucleophilic nitrogen atom N(6) to a metal centre has only recently been observed for the first time for triazaphospholes and is apparently enforced by the chelate effect.^[5] In agreement with our $\omega\text{B97xD}/6-31 + \text{G}^*$ calculations (by using the def2-TZVP basis at Re) on **7a**, the **K**-type structure is more stable than structure **J** by 9.9 kcal mol^{-1} . This stability difference is essentially due to the preferred binding of rhenium to nitrogen. In accordance, a P-bound mono-coordinated $[\text{Re}(\text{CO})_4\text{Br}]$ complex of *tert*-butyltriazaphosphole as a model is less stable than its N bound isomer by 12.4 kcal mol^{-1} at the $\omega\text{B97xD}/6-31 + \text{G}^*$ level (def2-TZVP basis at Re). Interestingly, the 1.336(13) Å bond length N(7)–C(14) is much shorter than the corresponding distance (C(1)–N(3)) in the free ligand **1a**. Also, the inter-ring distance N(5)–C(15) shortens significantly upon coordination (1.413(12) versus 1.436(2) Å). These differences nicely correlate with the shape of the LUMO of **1a** (see Figure S5 in the Supporting Information), which has a significant bonding character between the two rings. Once the ligand is coordinated to an electron-rich transition-metal centre, the low-lying ligand LUMO gains electron density, which results in an increase of the bond order and a shortening of the C(15)–N(5) bond.

To compare the stereoelectronic properties of triazaphosphole **1a** with triazole **6a**, a Re^I complex containing the chelating triazole was prepared accordingly. Since a phosphorus probe was absent, the reaction of **6a** with an equimolar amount of $[\text{Re}(\text{CO})_5\text{Br}]$ in dichloromethane at $T = 80^\circ\text{C}$ was monitored by means of ^1H NMR spectroscopy until full consumption of the ligand was observed. Crystals of **8a** (space group $P21/c$), suitable for XRD, were obtained by slowly cooling a concentrated solution of **8a** in dichloromethane. The molecular structure, along with selected bond lengths and angles, is depicted in Figure 12.

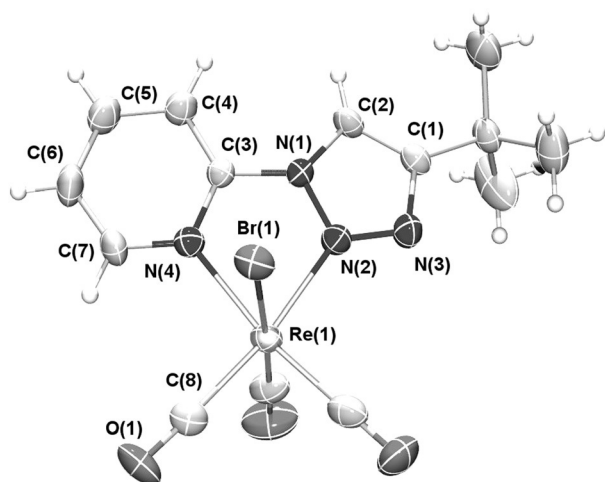


Figure 12. Molecular structure of a crystal of **8a**. Displacement ellipsoids are shown at the 50% probability level. A non-coordinated CH_2Cl_2 solvent molecule is omitted for clarity. Selected bond lengths [Å] and angles [$^\circ$]: C(2)–C(1): 1.365(7), C(2)–N(1): 1.356(6), N(1)–N(2): 1.352(6), N(2)–N(3): 1.313(5), N(3)–C(1): 1.367(6), N(1)–C(3): 1.417(6), N(4)–Re(1): 2.189(4), N(2)–Re(1): 2.146(4); N(4)–Re(1)–N(2): 73.93(15).

Similar to compound **7a**, the graphical representation of **8a** reveals the facial geometry of complex $[(\mathbf{6a})\text{Re}(\text{CO})_3\text{Br}]$ with nitrogen atom N(2) of the triazole units coordinated to the Re^I centre. Apparently, exchanging the phosphorus atom in **7a** for an isoelectronic C–H group in **8a** has only a marginal effect on the bite angle N(4)– Re^I –N(2), since values of 83.31° (**7a**) and 82.48° (**8a**) were found. Likewise, the N–Re distances are virtually unchanged. These observations are again in agreement with the carbon–phosphorus analogy.

Nevertheless, the changes in the bond lengths upon coordination of **6a** to the Re^I fragment are not as pronounced as those observed for phosphorus derivative **1a**. The N(3)–C(1) and inter-ring N(1)–C(3) distances in **8a** (1.367(6) and 1.417(6) Å, respectively) are only slightly shorter than those in free ligand **1a** (1.3704(16) and 1.4273(16) Å). The π -accepting character of **6a** seems to be much less pronounced than that of the phosphorus analogue **1a**.

To probe this, we further investigated the Re^I complexes **7a** and **8a** by means of IR spectroscopy and Table 3 provides a summary of the observations made.

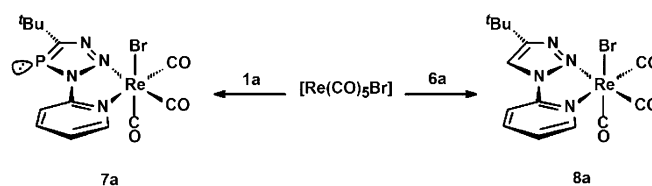
From the results in Table 3, it is clear that $\tilde{\nu}_2$ and $\tilde{\nu}_3$, in particular, in the triazaphosphole-based complex **7a** are shifted sig-

	$\tilde{\nu}_1(\text{CO})$ [cm^{-1}]	$\tilde{\nu}_2(\text{CO})$ [cm^{-1}]	$\tilde{\nu}_3(\text{CO})$ [cm^{-1}]
7a (tBu/P)	2023	1992	1900
8a (tBu/N)	2026	1913	1870

nificantly to higher wavenumbers relative to triazole-based Re^I complex **8a**. This is in agreement with the observations made above and indicates that triazaphosphole **1a** has a higher π -accepting capacity than that of **6a**. However, this is in clear contrast to the observations made for the non-conjugated, methylene-bridged triazaphospholes of type **B** (Figure 1), for which an inverse situation was observed.^[5]

Apparently, conjugation between the pyridyl and triazaphosphole moieties considerably affects the electron density of the phosphorus heterocycle in such way that the π -acceptor properties are increased, although differences in the steric constraints might also play a role.

During the preparation of our manuscript, Crowley et al. reported the crystallographic characterisation of the first Re^I complexes containing inverse phenyl- and benzyl-substituted 2-pyridyltriazole ligands. The bond lengths and angles reported for those coordination compounds are very similar to those observed for complex **8a** (Scheme 4).^[9a]



Scheme 4. Synthesis of Re^I complexes **7a** and **8a** from $[\text{Re}(\text{CO})_5\text{Br}]$.

Scheme 4 provides a summary of the reaction of ligands **1a** and **6a** with $[\text{Re}(\text{CO})_5\text{Br}]$, leading to the corresponding Re^I complexes **7a** and **8a**, in which coordination exclusively through the least nucleophilic nitrogen atom N(2) occurs.^[22]

Photophysical properties

To establish the structure–property relationship for this novel series of P-based π -conjugated systems (Figure 3), we started to investigate the photophysical properties of triazaphospholes **1a/b–3a** in comparison with reference compounds **4a/b** and **5a/b**, phosphorus-lacking triazoles **6a/b** and Re^I complexes **7a** and **8a**. The luminescence measurements were performed in dichloromethane at room temperature and the results are listed in Table 4 (see also Figures S6–S12 in the Supporting Information).

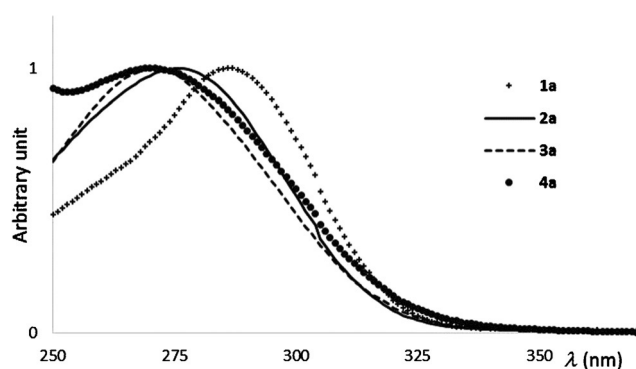
The absorption spectra of triazaphosphole derivatives **1a/b**, **2a/b**, **3a** and **4a/b** exhibit broad, medium-intensity bands in the UV part of the spectrum (see Figure 13 and Table 4). The $\omega\text{B97xD/aug-ccPVDZ}$ TD-DFT calculations performed on **1a/b**, **2a/b** and **3a/3b** at their minimum energy structures (see

Table 4. Photophysical features of the prepared compounds.

	$\lambda_{\text{max}}^{\text{[a]}}$ [nm]	ϵ [L mol ⁻¹ cm ⁻¹]	λ_{em} [nm]	Φ [%] ^[b]
1 a	285	3800	370	12
1 b	290	1900	334	11
2 a	275	9400	370	3
2 b	278	6700	338	— ^[c]
3 a	271	5900	360	0.4
4 a	270	9300	371	8
4 b	268	6800	—	— ^[d]
5 a	261	3900	—	— ^[d]
5 b	258	5400	—	— ^[d]
6 a	276	21 400	—	— ^[d]
6 b	275	11 300	—	— ^[d]
7 a	295	12 200	365	1.4
8 a	420	3100	—	—
	266	14 900	591	15 ^[e]
	379	4700	—	—

[a] Measured in CH₂Cl₂. [b] Fluorescence quantum yields were measured relative to quinine sulfate (H₂SO₄, 0.1 M), $\pm 15\%$. [c] The compound is not stable and undergoes decomposition. [d] Not determined; this emission was too low. [e] Emission quantum yields were measured relative to [Ru(bpy)]₃²⁺ in H₂O, $\varphi[\text{Ru}(\text{bpy})_3]^{2+} = 4.2\%$.

above) allow us to assign this feature to four electronic transitions (Table S1 in the Supporting Information). At higher wavelengths, a very low intensity ($f=0.002\text{--}0.02$) $\pi^*\text{--}n$ transition (mainly HOMO–3–LUMO) is predicted, typically between $\lambda=270$ and 280 nm for *t*Bu derivatives and $\lambda=280\text{--}290$ nm for SiMe₃ derivatives. Three further transitions are predicted in a 10 nm range at around $\lambda=250$ nm. One of them has a high HOMO–LUMO contribution and it also has about one order of magnitude higher calculated oscillator strength ($f=0.2\text{--}0.3$) than the other two. Apparently, this transition determines the observed spectrum. Indeed, the position of this intense transition is redshifted by $\lambda=8$ nm for **1 a** with respect to **2 a** and **3 a**, in accordance with the $\lambda=10$ nm redshift in the spectra shown in Figure 13. The redshift for **1 a/1 b** indicates increased π conjugation, in accordance with increased planarity (see below).

**Figure 13.** Normalised UV/Vis absorption spectra of compounds **1 a**, **2 a**, **3 a** and **4 a** in CH₂Cl₂ at room temperature.

Illumination of compounds **1 a/1 b** gave rise to a significant fluorescence emission with quantum yields of 12 and 11%. Exchange of the *t*Bu group for a SiMe₃ substituent results in a blueshift as the emission wavelength changes from $\lambda=370$ to 334 nm with a marginal effect on the quantum yield. In this respect, it is noteworthy that, likewise for **1 a**, our calculated structure for **1 b** was planar, and the rotational potential energy surface was also similar to that of **1 a**. The blueshift is much smaller in case of the absorption band maximum; nevertheless, it might be in agreement with the π -electron-withdrawing character of the --SiMe_3 group bonded directly to an aromatic system. Clearly, the planarity of **1 a** is related to the high quantum yield. Accordingly, the non-planar 3-pyridyl derivative (**2 a**) shows little fluorescence. Unexpectedly, however, the 4-pyridyl-substituted triazaphosphole **3 a**, which exhibits a planar X-ray structure, is very weakly emissive. To understand this behaviour, the rotational energy profile shown in Figure 7 should be considered. The rotational energy profile is steep in the case of **1 a**, whereas it is much shallower for both **2 a** and **3 a**; this makes the last two systems more flexible, which facilitates the radiationless deactivation of the excited state.

Exchange of the pyridyl functionality for a phenyl group in *t*Bu-substituted reference compound **4 a** leads to a low quantum yield compared with that of **1 a**; furthermore, replacing the *t*Bu group for a SiMe₃ substituent in **4 b** results in no emission at all. Also, the benzyl-substituted reference compounds **5 a/b** show no emission, which is apparently related to the lack of conjugation between the aryl group and triazaphosphole moiety.

Most interestingly, however, we found that the triazoles **6 a/ b** again had no emission at all, in contrast to structurally related 2-pyridyl-triazaphospholes **1 a/b**. This observation is striking, since the rotational surface, and consequently, the preference for planarity of the conjugated π system, was similar for the two molecules. Thus with similar behaviour in the ground state, we decided to investigate the geometry of the first excited state, which is of importance from the point of view of emission. Time-dependent (TD) B3LYP/cc-PVTZ geometry optimisations of the first excited state converged (depending on the starting geometry) to two planar structures for both **1 a** and **6 a**. Interestingly, however, although for phosphorus-containing fluorescent **1 a** the arrangement of the two rings is the same as that in the ground state (*cis*-NCNP structure), in the case of **6 a** the more stable excited-state geometry differs from the ground state by a rotation of 180° (Figure 14). Because fluorescence proceeds from the lowest excited state, and is governed by Frank–Condon factors, it is completely understandable that the difference in the ground- and excited-state geometries of **6 a** results in a low probability of emission.

If these results are translated to photophysical observations, a coplanar arrangement of the two heterocycles seems to be necessary for good emission properties, as indeed observed for **1 a**. The coplanar arrangement as the minimum structure points to a maximum degree of delocalisation within the π -conjugated system and is also observed in the molecular structure of **1 a** in the crystal (Figure 5). In contrast, compound **2 a** (3-pyridyl) shows very little emission and this compound has

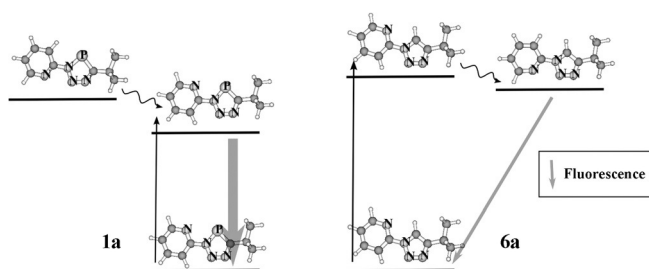


Figure 14. Schematic representation of the TD-DFT-optimised excited states and the ground-state geometries of **1a** and **6a**. The thickness of the arrows is related to the probability of the transition.

a twisted structure, according to XRD analysis (Figure 7) and our DFT calculations (see above). The calculations predict a twisted conformation as the minimum structure, with reduced conjugation. From the calculated data summarised in Table 2, a twisted conformation as the minimum structure is also predicted, which again is in agreement with reduced conjugation. The molecular structure of **3a** in the crystal, however, revealed a coplanar alignment of both heterocycles in the solid state. Nevertheless, as already mentioned above, this arrangement could be due to packing effects, which result in a coplanar arrangement of the two heterocycles in the crystal-line phase in an otherwise flexible system (Figure 8).

Next, we investigated the photophysical properties of the Re^I complexes **7a** and **8a**. The electronic absorption and emission spectra were recorded in CH_2Cl_2 at room temperature and are shown in Figure 15. The absorption spectrum of **8a** shows similar absorption bands to those of rhenium complexes reported previously.^[9a] The absorption spectrum presents an intense intra-ligand charge-transfer (ILCT) band centred at $\lambda = 266$ nm, along with a redshifted, broad and less intense metal to ligand charge-transfer (MLCT) band tailing down to $\lambda = 450$ nm (Figure 15). The MLCT band maximum is centred at $\lambda = 379$ nm, which is similar to the corresponding rhenium complex that incorporates 2-(4-phenyl-1*H*-1,2,3-triazol-1-yl)pyridine as a ligand. This behaviour indicates that the substituent on the triazole ring (phenyl versus *t*Bu) is not involved in the MLCT transition.^[9a]

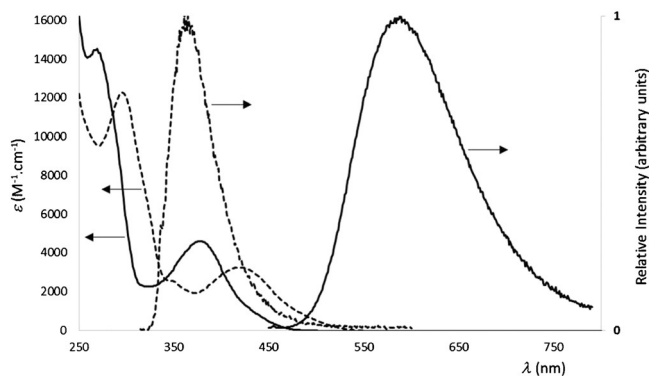


Figure 15. Electronic absorption and emission spectra for the Re^I complexes **7a** (dashed lines) and **8a** (solid lines) in CH_2Cl_2 at room temperature.

Replacement of the CH unit by P in the five-membered ring (complex **7a**; Figure 15) results in a redshift of the absorption band maxima. The spectrum of **7a** presents an intense band centred at $\lambda = 295$ nm, along with a redshifted shoulder and the MLCT feature (band maximum at $\lambda = 420$ nm) tailing down to $\lambda = 525$ nm (Figure 15).

To rationalise the observed properties, DFT and TD-DFT calculations were carried out on complexes **7a** and **8a**. Analysis of the molecular orbitals of complexes **7a** and **8a** shows that the orbitals between HOMO and HOMO-5 are mainly localised at the $\{\text{Re}(\text{CO})_3\text{Br}\}$ fragment and have similar energies and shapes for the two related molecules (see Figures S13 and S14 in the Supporting Information). In contrast, the LUMO (see Figure S13 and S14 in the Supporting Information) is localised at the ligand core, and is stabilised by 0.5 eV in **7a** with respect to **8a**. Furthermore, the LUMO exhibits significant pyridine character for complex **8a** and triazaphosphole character for complex **7a**. This behaviour is in accordance with the known stabilisation of the $\pi^*_{\text{P}=\text{C}}$ energy levels with respect to their $\pi^*_{\text{C}=\text{C}}$ counterparts, as shown by a comparative investigation of the electron transmission spectra of the corresponding benzene, phosphabenzene and triphosphabenzene derivatives.^[23,24]

The TD-DFT computations performed on complexes **7a** and **8a** predict 15 transitions for both complexes at wavelengths higher than $\lambda = 250$ nm. Most of these transitions are of low intensity ($f = 0.0001\text{--}0.02$); thus having only a small contribution to the spectrum. There are three features, however, that have higher intensity and we assign those to the observed band maxima. The corresponding transitions are LUMO \leftarrow HOMO-1 at $\lambda = 444$ nm ($f = 0.0607$) for **7a** and $\lambda = 394$ nm ($f = 0.053$) for **8a**; these can be assigned to the $\lambda = 420$ and 379 nm MLCT bands, respectively. Also, the transition at $\lambda = 310$ nm ($f = 0.0762$) of **7a** may be assigned to the shoulder at $\lambda \approx 350$ nm in the spectrum. The corresponding transition for **8a** is at $\lambda = 285$ nm ($f = 0.0645$). These transitions belong to an excitation from a metal $d\text{--}\pi(\text{CO})$ bonding orbital to the LUMO. The third intense pairs of transitions are located at $\lambda = 263$ ($f = 0.2147$) and 250 nm ($f = 0.0668$) for **7a** and **8a**, respectively. These transitions are due to $\pi^*\text{--}\pi$ excitations of the ligand. Because all of these dominant transitions belong to excitations to the LUMO, their energy shift between **7a** and **8a** should be related to the energy difference of the LUMOs of the ligands. Accordingly, the LUMO level for complex **7a** is more stabilised than the LUMO level of complex **8a**, as discussed above.

Illumination of complexes **7a** and **8a** in deoxygenated CH_2Cl_2 at the maximum of the MLCT band gave rise to phosphorescence emission with a maximum centred at $\lambda = 591$ nm for compound **8a** only. No triplet emission was observed for compound **7a** (Table 4). Moreover, no further emissions were detected at low temperature. These photophysical data indicate that radiation-less deactivation pathways are mainly responsible for the deactivation of the MLCT excited states for complex **7a**.

The excitation of complex **8a** at the maximum of the ILCT band gave rise to the triplet emission centred at $\lambda = 591$ nm, which indicated efficient relaxation to the $^3\text{MLCT}$ excited state.

Most interestingly, compound **7a** shows different behaviour when it is excited at $\lambda = 295$ nm (at the ILCT band). A fluorescent emission centred at $\lambda = 365$ nm is recorded, which resembles ligand fluorescence. These results indicate that energy transfer from the ILCT state to the MLCT band is not efficient.

Currently, a straightforward explanation for the emissive properties of complex **7a** remains elusive. However, the major difference between complexes **7a** and **8a** lies in the localisation of the electron density in the LUMO level. The DFT calculations showed that the LUMO of complex **7a** had an important triazaphosphole character with a strong contribution from the phosphorus atom because complex **8a** had strong electron density on pyridine, which indicated different deactivation pathways for the MLCT excited state. Experiments to clarify this aspect are currently being performed in our laboratories.

Conclusion

Due to the modular synthetic procedure for the preparation of 3*H*-1,2,3,4-triazaphosphole derivatives, we demonstrated, for the first time, access to pyridyl-functionalised triazaphospholes with either *t*Bu or SiMe₃ substituents at the 5-position of the N₃PC heterocycle. The *t*Bu-substituted compounds were characterised by means of X-ray crystal-structure analysis, which demonstrated significant differences in the torsion angles between the two heterocycles. DFT calculations showed that the rotation of the two rings was more hindered in the 2-pyridyl-substituted triazaphosphole than in its 3- and 4-pyridyl-substituted analogues. To compare the 2-pyridyl-functionalised triazaphospholes, in particular, with the corresponding phosphorus-lacking systems, 2-pyridyl-functionalised triazole derivatives were prepared and structurally characterised. Starting from [Re(CO)₅Br], it turned out that the chelating triazaphospholes formed complexes of the type [(N[∧]N)Re(CO)₃Br], with the pyridyl nitrogen and least nucleophilic nitrogen atom N(6) of the triazaphosphole moiety bound to the Re^I atom, rather than through the phosphorus atom. Both structural and IR spectroscopic investigations of the Re^I-carbonyl complexes revealed that the chelating triazaphosphole had a significantly higher π -accepting capacity than the structurally related triazole derivative. Irradiation of the 2-pyridyl-substituted triazaphospholes gave rise to a significant fluorescence emission, whereas the structurally related triazole (*t*Bu) showed no emission at all. In this respect, there was a clear influence of the phosphorus atom on the photophysical properties of the corresponding compounds. We further found that the emission capability of the triazaphospholes strongly depended on the position of the nitrogen atom within the pyridine heterocycle. To explain the experimental findings, DFT calculations were performed, the results for which suggested that a coplanar arrangement of the two heterocycles was a necessary prerequisite for good emission properties, as indeed observed for the 2-pyridyl-functionalised triazaphosphole. However, a planar structure as an energy minimum might also exist in a flexible structure (e.g., in **3a**), resulting in bad emission properties. A further important observation was that matching of the ground- and excited-state rotational energy surfaces was also of importance for

good emissive properties. We showed that, although 2-pyridyl-substituted triazole **6a** had a similarly rigid structure to its analogue **1a**, since its excited-state conformational preference differed from that of the ground state, its emissive properties were much less favourable. Our experimental and theoretical findings establish, for the first time, triazaphospholes as a new class of phosphorus-containing extended π systems. Further experiments are currently being undertaken to optimise the structure of π -conjugated systems that incorporate triazaphospholes to generate visible emissions for future optoelectronic applications.

Experimental Section

General

All reactions were performed in an argon atmosphere by using Schlenk techniques, unless stated otherwise. All glassware was dried prior to use by heating under vacuum. All common chemicals were commercially available and purchased from Aldrich Chemical Co., ABCR, Alfa Aesar or Acros, as well as Eurisol, and were used as received. All solvents were dried and degassed by using standard techniques or used as directly obtained from Braun Solvent systems. The ¹H, ¹³C{¹H} and ³¹P{¹H} NMR spectra were recorded on JEOL ECX400 (400 MHz), JEOL ECP500 (500 MHz), Bruker AVANCE500 (500 MHz), or Bruker AVANCE700 (700 MHz) spectrometers, and all chemical shifts were reported relative to the residual resonance in the deuterated solvents. IR spectra were obtained by using a Nicolet iS10 MIR FTIR spectrometer. Arylbromides (Aryl = Ph, 2-Py, 3-Py, 4-Py) were obtained from Acros Organics and Sigma Aldrich, and were used without any additional purification. Rhenium pentacarbonyl bromide was purchased from ABCR. ESI-TOF-MS was performed on an Agilent 6210 ESI-TOF instrument, Agilent Technologies, Santa Clara, CA, USA (5 μ L min⁻¹, 4 kV, 15 psi). The voltage was optimised during measurements of the maximum abundance of the [M + X] signal (X: H, Na, K). Microwave reactions were performed with an Anton Paar Monowave 300 microwave.

DFT calculations

DFT calculations were carried out with the Gaussian 09 suite of programs.^[25] Geometry optimisation was performed at the ω B97xD/aug-cc-pVTZ level^[26] to account for dispersion effects, which were likely to contribute significantly to interactions that influenced the rotational energy surface. The complexes were calculated at the ω B97xD/6-31 + G* level (for the transition metals, the def2-TZVP basis set was used). Geometries were fully optimised and at the minima second derivatives were calculated to ensure that real minima were obtained. To find the rotational energy surfaces, relaxed scan calculations were carried out at 30° intervals. The computed molecular structures and orbitals were visualised by means of the MOLDEN program.^[27]

General synthetic procedure for aryl azides

Aryl azides were synthesised by using a related protocol reported by Liang et al.^[28] The corresponding bromide (10 mmol) was dissolved in a degassed mixture of water/EtOH (100 mL; 7:3 v/v). Sodium azide (2 equiv), copper iodide (10 mol%) and *N,N*-dimethylethylenediamine (30 mol%) were added. The reaction mixture was heated at reflux under an argon atmosphere for 2 h, cooled to RT and diluted with H₂O (50 mL). The organic compounds were ex-

tracted by washing with Et₂O (3 × 100 mL), and the combined organic phases were washed with brine, dried over MgSO₄, concentrated and filtered through a SiO₂ plug (ϕ = 6.5 cm × 3 cm). The solvent was removed in vacuo and the crude products were used without additional purification. There was one exception (see below): tetrazolo[1,5-*a*]pyridine **F** ("2-azido pyridine", see above) was purified by column chromatography (SiO₂, dichloromethane/ethyl acetate 9:1 v/v).

Compound 1a

Tetrazolo[1,5-*a*]pyridine (450.0 mg, 3.75 mmol, 1 equiv) was added to a solution of (2,2-dimethylidene)phosphine (412.9 mg, 4.13 mmol, 1.5 equiv) in toluene (30 mL). The reaction mixture was heated for 1 week at *T* = 80 °C. After full conversion of the starting material, the solvent and excess (2,2-dimethylpropylidene)phosphine were removed in vacuo. The crude product was redissolved in toluene at RT and crystallised by slow cooling to *T* = -20 °C. Compound **1a** was obtained as slightly yellow needles (437.7 mg, 1.99 mmol, 53%). ¹H NMR (400 MHz, CD₂Cl₂): δ = 1.48 (d, ⁴*J*(H,P) = 1.6 Hz, 9H; Me-H9, Me-H10, Me-H11), 7.31 (ddd, ³*J*(H,H) = 7.5 Hz, ³*J*(H,H) = 4.9 Hz, ⁴*J*(H,H) = 1.1 Hz, 1H; Ar-H5), 7.88 (td, ³*J*(H,H) = 7.8 Hz, ⁴*J*(H,H) = 1.9 Hz, 1H; Ar-H4), 8.08 (dt, ³*J*(H,H) = 8.3 Hz, ⁴*J*(H,H) = 1.0 Hz, 1H), 8.44 ppm (ddd, ³*J*(H,H) = 4.9 Hz, ⁴*J*(H,H) = 1.9 Hz, ⁵*J*(H,H) = 0.9 Hz, 1H; Ar-H6); ¹³C NMR (176 MHz, CD₂Cl₂): δ = 31.1 (d, ³*J*(C,P) = 8.3 Hz; Me-C8, Me-C9, Me-C10), 35.3 (d, ²*J*(C,P) = 15.3 Hz; *t*Bu-C7), 113.4 (d, ³*J*(C,P) = 2.6 Hz; Ar-C3), 123.5 (s; Ar-C5), 139.1 (s; Ar-C4), 148.5 (s; Ar-C6), 153.3 (d, ²*J*(C,P) = 8.4 Hz; Ar-C2), 199.0 ppm (d, ¹*J*(C,P) = 57.2 Hz; Ar-C1); ³¹P{¹H} NMR (162 MHz, CD₂Cl₂): δ = 167.51 ppm; HR-ESI-TOF-MS (+, 150.0 V): *m/z* calcd for C₁₀H₁₃N₄P [M + H]⁺: 221.0951; found: 221.0967; elemental analysis calcd (%) for C₁₀H₁₃N₄P: N 25.44, C 54.54, H 5.95; found: N 25.36, C 54.56, H 5.97.

General synthesis of compounds 2a–5a

Aryl and benzyl azides (3.75 mmol) were mixed with a stirring bar in a 100 mL Normag flask. Subsequently, the azide was frozen and the flask was evacuated, followed by the addition of dry toluene (≈ 50 mL) and (dimethylidene)phosphine (412.9 mg, 4.13 mmol, 1.5 equiv). The reaction solution was allowed to warm to RT and was stirred for 24 h. The solvent and excess alkyne were removed in vacuo. The resulting solid was recrystallised from a hot saturated solution in *n*-pentane.

Compound 2a: White crystalline needles (668.89 mg, 3.04 mmol, 81%); ¹H NMR (400 MHz, CD₂Cl₂): δ = 1.51 (d, ⁴*J*(H,P) = 1.5 Hz, 9H; *t*Bu), 7.47 (ddd, ³*J*(H,H) = 8.2 Hz, ³*J*(H,H) = 4.8 Hz, ⁴*J*(H,H) = 0.8 Hz, 1H; Ar-H4), 8.12 (dddd, ³*J*(H,H) = 8.2 Hz, ⁴*J*(H,P) = 2.5, ⁴*J*(H,H) = 1.5 Hz, ⁵*J*(H,H) = 1.0 Hz, 1H; Ar-H3), 8.65 (dd, ³*J*(H,H) = 4.8 Hz, ⁴*J*(H,H) = 1.5 Hz, 1H; Ar-H5), 9.03 ppm (dt, ⁴*J*(H,P) = 2.3 Hz, ⁴*J*(H,H) = 1.0 Hz, 1H; Ar-H6); ¹³C NMR (101 MHz, CD₂Cl₂): δ = 31.2 (d, ³*J*(C,P) = 7.9 Hz; Me-C8, Me-C9, Me-C10), 35.4 (d, ²*J*(C,P) = 15.5 Hz; *t*Bu-C7), 124.1 (s; Ar-C4), 129.4 (d, ³*J*(C,P) = 6.0 Hz; Ar-C3), 137.5 (d, ²*J*(C,P) = 9.4 Hz; Ar-C2), 143.4 (d, ³*J*(C,P) = 8.6 Hz; Ar-C7), 149.7 (s; Ar-C5), 199.0 ppm (d, ¹*J*(C,P) = 56.5 Hz; Ar-C1); ³¹P{¹H} NMR (162 MHz, CD₂Cl₂): δ = 170.9 ppm (s); HR-ESI-TOF-MS (+, 250.0 V): *m/z* calcd for C₁₀H₁₃N₄P [M + H]⁺: 221.0951; found: 221.0969; elemental analysis calcd (%) for C₁₀H₁₃N₄P: N 25.44, C 54.54, H 5.95; found: N 25.50, C 54.51, H 5.89.

Compound 3a: White crystalline needles (685.4 mg, 3.11 mmol, 83%); ¹H NMR (500 MHz, CD₂Cl₂): δ = 1.51 (d, ⁴*J*(H,P) = 1.7 Hz, 9H; Me-H8, Me-H9, Me-H10), 7.79 (dt, ³*J*(H,H) = 4.6 Hz, ⁴*J*(H,P) = 1.4 Hz, 2H; Ar-H4, Ar-H5), 8.70 ppm (m, 2H; Ar-H3, Ar-H6); ¹³C NMR (176 MHz, CD₂Cl₂): δ = 31.6 (d, ³*J*(C,P) = 8.1 Hz; Me-C8, Me-C9, Me-

C10), 36.0 (d, ²*J*(C,P) = 15.5 Hz; *t*Bu-C7), 116.1 (d, ³*J*(C,P) = 8.3 Hz; Ar-C3, Ar-C6), 147.8 (d, ²*J*(C,P) = 11.4 Hz; Ar-C2), 152.1 (s; Ar-C4, Ar-C5), 199.8 ppm (d, *J* = 55.4 Hz; Ar-C1); ³¹P{¹H} NMR (162 MHz, CD₂Cl₂): δ = 174.7 ppm (s); HR-ESI-TOF-MS (+, 150.0 V): *m/z* calcd for C₁₀H₁₃N₄P [M + H]⁺: 221.0951; found: 221.0965; elemental analysis calcd (%) for C₁₀H₁₃N₄P: N 25.44, C 54.54, H 5.95; found: N 25.76, C 54.41, H 5.84.

Compound 4a: White crystalline solid (715.21 mg, 3.26 mmol, 87%); ¹H NMR (400 MHz, CD₂Cl₂): δ = 1.49 (d, ⁴*J*(H,P) = 1.5 Hz, 9H; Me-H9, Me-H10, Me-H11), 7.42 (m, 1H; Ar-H5), 7.48 (m, 2H; Ar-H4, Ar-H6), 7.76 ppm (m, 2H; Ar-H3, Ar-H7); ¹³C NMR (176 MHz, CD₂Cl₂): δ = 31.8 (d, ³*J*(C,P) = 7.6 Hz; Me-C9, Me-C10, Me-C11), 35.9 (d, ²*J*(C,P) = 16.2 Hz; *t*Bu-C8), 122.8 (d, ³*J*(C,P) = 7.3 Hz; Ar-C3, Ar-C7), 129.0 (s; Ar-C5), 130.1 (s; Ar-C4, Ar-C6), 141.6 (d, ²*J*(C,P) = 10.4 Hz; Ar-C2), 199.0 ppm (d, ¹*J*(C,P) = 55.5 Hz; Ar-C1); ³¹P{¹H} NMR (162 MHz, CD₂Cl₂): δ = 174.3 ppm (s); HR-ESI-TOF-MS (+, 200.0 V): *m/z* calcd for C₁₁H₁₄N₃P [M + H]⁺: 220.0998; found: 220.1013; elemental analysis calcd (%) for C₁₁H₁₄N₃P: N 19.17, C 60.27, H 6.44; found: N 18.59, C 60.06, H 6.46.

Compound 5a: White crystalline solid (776.39 mg, 3.30 mmol, 88%); ¹H NMR (500 MHz, CD₂Cl₂): δ = 1.43 (d, ⁴*J*(H,P) = 1.6 Hz, 9H; Me-H), 5.69 (d, ³*J*(H,P) = 6.8 Hz, 2H; CH₂), 7.36 ppm (m, 5H; Ar-H); ¹³C NMR (176 MHz, CD₂Cl₂): δ = 31.9 (d, ³*J*(C,P) = 8.0 Hz; Me-C10, Me-C11, Me-C12), 35.7 (d, ²*J*(C,P) = 16.2 Hz; *t*Bu-C9), 56.6 (d, ²*J*(C,P) = 13.0 Hz; CH₂-C2), 128.9 (s; Ar-C5, Ar-C7), 129.0 (s; Ar-C6), 129.4 (s; Ar-C4, Ar-C8), 137.9 (d, ⁴*J*(C,P) = 1.9 Hz; Ar-C3), 199.3–198.2 ppm (d, ¹*J*(C,P) = 56.3 Hz; Ar-C1); ³¹P{¹H} NMR (162 MHz, CD₂Cl₂): δ = 171.4 ppm (s); HR-ESI-TOF-MS (+, 200 V): *m/z* calcd for C₁₂H₁₆N₃P [M + H]⁺: 234.1155; found: 234.1151; elemental analysis calcd (%) for C₁₂H₁₆N₃P: N 18.02, C 61.79, H 6.91; found: N 17.79, C 61.79, H 6.91.

General synthesis procedure of 5-TMS-substituted triaza-phospholes

Aryl and benzyl azides (3.75 mmol) were mixed with a stirring bar in a 250 mL Normag flask. Subsequently, the azide was frozen and the flask was evacuated, followed by the addition of dry [(trimethylsilyl)methylidene]phosphine (≈ 100 mL) in toluene (large excess). The reaction solution was allowed to warm to RT and was stirred for 24 h. The solvent and excess alkyne were removed in vacuo.

Compound 1b: Orange oil (806.34, 3.41 mmol, 91%); ¹H NMR (400 MHz, CD₂Cl₂): δ = 8.49 (ddd, *J* = 4.9, 1.8, 0.9 Hz, 1H; H_{Ai}), 8.14 (dt, *J* = 8.2, 0.9 Hz, 1H; H_{Ai}), 7.95–7.89 (m, 1H; H_{Ai}), 7.35 (ddd, *J* = 7.4, 4.9, 1.0 Hz, 1H; H_{Ai}), 0.44 ppm (d, *J* = 0.6 Hz, 9H; CH₃); ¹³C NMR (101 MHz, CD₂Cl₂): δ = 186.4 (d, ¹*J*(P,C) = 74.0 Hz; C=P), 153.6 (d, ²*J*(P,C) = 7.1 Hz; C_{2, Ar}), 149.2, 139.8 (s; C_{Ar}), 124.2 (d, ⁴*J*(P,C) = 1.1 Hz; C_{4, Ar}), 114.6 (d, ³*J*(P,C) = 2.2 Hz; C_{3, Ar}), -0.19 ppm (d, ³*J*(P,C) = 3.8; CH₃); ³¹P{¹H} NMR (162 MHz, CD₂Cl₂): δ = 211.6 ppm (s).

Compound 2b: Orange solid (824.1 mg, 3.49 mmol, 93%); ¹H NMR (400 MHz, CD₂Cl₂): δ = 9.14–8.99 (m, 1H; H_{Ai}), 8.66 (dd, *J* = 4.8, 1.4 Hz, 1H; H_{Ai}), 8.17–8.12 (m, 1H; H_{Ai}), 7.48 (ddt, *J* = 8.2, 4.8, 0.8 Hz, 1H; H_{Ai}), 0.45 ppm (s, 9H; CH₃); ¹³C NMR (101 MHz, CD₂Cl₂): δ = 186.4 (d, ¹*J*(P,C) = 75.5 Hz; C=P), 150.3 (d, ⁴*J*(P,C) = 1.2 Hz; C_{5, Ar}), 144.1 (d, ²*J*(P,C) = 7.7 Hz; C_{3, Ar}), 130.2 (d, ³*J*(P,C) = 5.3 Hz; C_{4, Ar}), 124.7 (s; C_{6, Ar}), -0.21 ppm (d, ³*J*(P,C) = 3.6 Hz; CH₃); ³¹P{¹H} NMR (162 MHz, CD₂Cl₂): δ = 213.7 ppm (s); HR-ESI-TOF-MS (+, 330 V): *m/z* calcd for C₉H₁₃N₄PSi [M + Na]⁺: 259.0539; found: 259.1177.

Compound 4b: Red oil (803.0 mg, 3.41 mmol, 91%); ¹H NMR (400 MHz, CD₂Cl₂): δ = 7.82 (dt, *J* = 8.4, 1.2 Hz, 2H; H_{Ai}), 7.55–7.50 (m, 2H; H_{Ai}), 7.48–7.42 (m, 1H; H_{Ai}), 0.46 ppm (d, *J* = 0.6 Hz, 9H; Me); ¹³C NMR (101 MHz, CD₂Cl₂): δ = 185.7 (d, ¹*J*(P,C) = 74.7 Hz; C=

P), 141.3 (d, $^2J(P,C) = 9.3$ Hz; $C_{1,Ar}$), 130.2 (s; $C_{4,Ar}$), 129.1 (d, $^4J(P,C) = 1.1$ Hz; $C_{3,3',Ar}$), 123.1 (d, $^3J(P,C) = 6.5$ Hz; $C_{2,2',Ar}$), -0.13 ppm (d, $^3J(P,C) = 3.6$ Hz; Me); $^{31}P\{^1H\}$ NMR (162 MHz, CD_2Cl_2): $\delta = 213.0$ ppm (s).

Compound 5b: White crystalline solid (876.5 mg, 3.49 mmol, 93%); 1H NMR (400 MHz, CD_2Cl_2): $\delta = 0.38$ (d, $^4J(H,P) = 0.5$ Hz, 9H; Me-H9, Me-H10, Me-H11), 5.81 (d, $^3J(H,P) = 6.0$ Hz, 2H), 7.37 ppm (m, 1H); ^{13}C NMR (101 MHz, CD_2Cl_2): $\delta = -0.13$ (d, $^3J(C,P) = 3.5$ Hz; Me-C9, Me-C10, Me-C11), 56.1 (d, $^2J(C,P) = 12.1$ Hz; CH_2-C2), 128.9 (d, $^4J(C,P) = 1.2$ Hz; Ar-C4, Ar-C5), 129.0 (s; Ar-C6), 129.4 (s; Ar-C5, Ar-C7), 137.9 (d, $^3J(C,P) = 2.0$ Hz; Ar-C3), 185.5 ppm (d, $^1J(C,P) = 74.8$ Hz; Ar-C1); ^{31}P NMR (162 MHz, CD_2Cl_2): $\delta = 214.7$ ppm (s); HR-ESI-TOF-MS (+, 200 V): m/z calcd for $C_{11}H_{16}N_3PSi$ [$M+H$] $^+$: 250.0924; found: 250.0909; elemental analysis calcd (%) for $C_{11}H_{16}N_3PSi$: N 16.85, C 52.99, H 6.47; found: N 16.67, C 52.69, H 6.48.

General synthesis of 1,2,3-triazoles

Copper(I) trifluoromethanesulfonate benzene complex (188.7 mg, 0.375 mmol, 10 mol%) was added to tetrazolo[1,5-*a*]pyridine (**F**; 450 mg, 3.75 mmol) in a 20 mL microwave reaction vessel. Dry toluene (20 mL) was added along with substituted alkyne (4.125 mmol, 1.1 equiv). The mixture was heated to 140 °C for 4 h in the microwave. After cooling the reaction vessel to RT, the solvent was removed in vacuo and column chromatography (SiO_2 , CH_2Cl_2 /ethyl ether 9:1 v/v) gave the pure title compounds.

Compound 6a: White solid (583.62 mg, 2.89 mmol, 77%); 1H NMR (500 MHz, $CDCl_3$): $\delta = 1.41-1.38$ (s, 9H; Me-H12, Me-H13, Me-H14), 7.29 (ddd, $^3J(H,H) = 7.4$ Hz, $^3J(H,H) = 4.9$ Hz, $^4J(H,H) = 1.0$ Hz, 1H; Ar-H6), 7.87 (ddd, $^3J(H,H) = 8.2$ Hz, $^3J(H,H) = 7.4$ Hz, $^4J(H,H) = 1.8$ Hz, 1H; Ar-H5), 8.16 (dt, $^3J(H,H) = 8.2$ Hz, $^4J(H,H) = 1.0$ Hz, 1H; Ar-H4), 8.27 (s, 1H; Ar-Triazol-H2), 8.46 ppm (ddd, $^3J(H,H) = 4.9$ Hz, $^4J(H,H) = 1.9$ Hz, $^5J(H,H) = 0.9$ Hz, 1H; Ar-H7); ^{13}C NMR (126 MHz, $CDCl_3$): $\delta = 30.3$ (s; Me-C12, Me-C13, Me-C14), 31.0 (s; tBu-C11), 113.9 (s; Ar-C4), 116.1 (s; Ar-Triazol-C2), 123.3 (s; Ar-C6), 139.2 (s; Ar-C5), 148.5 (s; Ar-C7), 149.6 (s; Ar-C3), 158.2 ppm (s; Ar-Triazol-C1); HR-ESI-TOF-MS (+, 100.0 V): m/z calcd for $C_{11}H_{14}N_4$ [$M+Na$] $^+$: 225.11107; found: 225.1126; elemental analysis calcd (%) for $C_{11}H_{14}N_4$: N 27.70, C 65.32, H 6.98; found: N 28.17, C 65.15, H 6.79.

Compound 6b: White solid (483.0 mg, 2.21 mmol, 59%); 1H NMR (500 MHz, $CDCl_3$): $\delta = 0.37$ (s, 9H; Me-H11, Me-H12, Me-H13), 7.32 (ddd, $^3J(H,H) = 7.4$ Hz, $^3J(H,H) = 4.9$ Hz, $^4J(H,H) = 1.0$ Hz, 1H; Ar-H6), 7.90 (ddd, $^3J(H,H) = 8.2$ Hz, $^3J(H,H) = 7.4$ Hz, $^4J(H,H) = 1.8$ Hz, 1H; Ar-H5), 8.20 (dt, $^3J(H,H) = 8.2$ Hz, $^4J(H,H) = 1.0$ Hz, 1H; Ar-H4), 8.49 (ddd, $^3J(H,H) = 4.9$ Hz, $^4J(H,H) = 1.9$ Hz, $^5J(H,H) = 0.9$ Hz, 1H; Ar-H7), 8.55 ppm (s, 1H; Ar-Triazol-H2); ^{13}C NMR (126 MHz, $CDCl_3$): $\delta = -1.1$ (s; Me-C12, Me-C13, Me-C14), 114.4 (s; Ar-C4), 123.4 (s; Ar-C6), 126.5 (s; Ar-Triazol-C2), 139.3 (s; Ar-C5), 147.3 (s; Ar-C3), 148.6 (s; Ar-C7), 149.5 ppm (s; Ar-Triazol-C1); HR-ESI-TOF-MS (+, 150.0 V): m/z calcd for $C_{10}H_{14}N_4Si$ [$M+Na$] $^+$: 241.0880; found: 241.0881; elemental analysis calcd (%) for $C_{10}H_{14}N_4Si$: N 25.66, C 55.01, H 6.46; found: N 25.59, C 54.92, H 6.52.

General synthesis of Re^I complexes

[Re(CO)₅Br] (50 mg, 0.123 mmol) was mixed with ligand **5a** or **6a** (0.123 mmol) in a Young NMR tube and suspended in dry CD_2Cl_2 (0.5 mL). The reaction mixture was heated for 8 h at 80 °C, leading to full conversion (as determined by $^1H/^{31}P$ NMR spectroscopy). The precipitated product was recrystallised by cooling a hot saturated solution of **7a** or **8a** slowly, yielding single-crystalline pure compounds.

Compound 7a: Red needles (44.2 mg, 0.08 mmol, 63%); 1H NMR (700 MHz, CD_2Cl_2): $\delta = 1.57$ (d, $^4J(H,P) = 1.5$ Hz, 9H; Me-H11, Me-H12, Me-H13), 7.35 (ddd, $^3J(H,H) = 7.3$ Hz, $^4J(H,H) = 5.6$ Hz, $^5J(H,H) = 1.1$ Hz, 1H; Ar-H5), 8.06 (d, $^3J(H,H) = 8.2$ Hz, 1H; Ar-H3), 8.16 (ddd, $^3J(H,H) = 8.2$ Hz, $^4J(H,H) = 7.6$ Hz, $^5J(H,H) = 1.7$ Hz, 1H; Ar-H4), 8.92 ppm (dd, $^3J(H,H) = 5.4$ Hz, $^4J(H,H) = 1.4$ Hz, 1H; Ar-H6); ^{13}C NMR (176 MHz, CD_2Cl_2): $\delta = 31.4$ (d, $^3J(C,P) = 9.1$ Hz; Me-C11, Me-C12, Me-C13), 36.7 (d, $^2J(C,P) = 14.6$ Hz), 116.7 (d, $^3J(C,P) = 13.5$ Hz; Ar-C3), 126.2 (s; Ar-C5), 142.3 (s; Ar-C4), 152.9 (s; Ar-C6), 153.0 (d, $^2J(C,P) = 10.0$ Hz), 188.1 (s; CO), 195.2 (s; CO), 197.1 (s; CO), 201.6 ppm (d, $^1J(C,P) = 60.9$ Hz), ^{31}P NMR (162 MHz, CD_2Cl_2): $\delta = 184.1$ ppm (s); HR-ESI-TOF-MS (+, 200 V): m/z calcd for $C_{13}H_{13}BrN_4O_3Pre$ [$M-Br+MeCN$] $^+$: 532.0543; found: 532.0583; elemental analysis calcd (%) for $C_{13}H_{13}BrN_4O_3Pre$: N 8.55, C 25.66, H 2.31; found: N 8.89, C 26.15, H 2.32; one molecule of CH_2Cl_2 is found in the lattice of the molecular structure in the crystal.

Compound 8a: Yellow needles (38.7 mg, 0.07 mmol, 57%); 1H NMR (700 MHz, $CDCl_3$): $\delta = 1.45$ (s, 9H; Me-H12, Me-H13, Me-H14), 7.35 (ddd, $J = 7.6, 5.6, 1.0$ Hz, 1H; Ar-H5), 7.81 (d, $^3J(H,H) = 8.2$ Hz, 1H; Ar-H4), 8.15 (s, 1H; Ar-Triazol-H2), 8.19 (ddd, $^3J(H,H) = 8.3$, $^4J(H,H) = 7.6$ Hz, $^5J(H,H) = 1.6$ Hz, 1H; Ar-H6), 8.97 ppm (ddd, $^3J(H,H) = 5.5$ Hz, $^4J(H,H) = 1.5$ Hz, $^5J(H,H) = 0.6$ Hz, 1H; Ar-H7); ^{13}C NMR (176 MHz, $CDCl_3$): $\delta = 30.1$ (s; Me-C12, Me-C13, Me-C14), 31.7 (s; tBu-C11), 113.2 (s; Ar-C4), 118.0 (s), 125.7 (s; Ar-C5), 142.0 (s; Ar-C6), 147.7 (s; Ar-C3), 153.3 (s; Ar-C7), 161.7 (s; Ar-C1), 187.6 (s; CO), 193.9 (s; CO), 195.9 ppm (s; CO); HR-ESI-TOF-MS (+, 150.0 V): m/z calcd for $C_{14}H_{14}BrN_4O_3Re$ [$M+Na$] $^+$: 574.9699; found: 574.9704; elemental analysis calcd (%) for $C_{14}H_{14}BrN_4O_3Re$: N 10.14, C 30.44, H 2.55; found: N 9.76, C 30.08, H 2.67.

X-ray crystal-structure determination of 1a

Crystals suitable for XRD were obtained by cooling a saturated solution of **1a** in toluene. Crystallographic data: $C_{10}H_{13}N_4P$; $M_r = 220.21$; $0.50 \times 0.37 \times 0.29$ mm³; colourless blocks; orthorhombic; $Pnma$; $a = 7.9500(10)$, $b = 6.8020(8)$, $c = 20.732(3)$ Å; $\alpha = 90$, $\beta = 90$, $\gamma = 90^\circ$; $V = 1121.1(3)$ Å³; $Z = 4$; $D_x = 1.305$ g cm⁻³; $\mu = 0.218$ mm⁻¹; 6647 reflections were measured by using a Stoe IPDS 2T diffractometer with a rotating anode ($Mo_{K\alpha}$ radiation; $\lambda = 0.71073$ Å) up to a resolution of $\sin \theta / \lambda_{max} = 0.69$ Å⁻¹ at a temperature of 210 K; 1607 reflections were unique ($R_{int} = 0.035$). The structures were solved with SHELXS-2013^[31] by using direct methods and refined with SHELXL-2013^[31] on F^2 for all reflections. Non-hydrogen atoms were refined by using anisotropic displacement parameters. The positions of the hydrogen atoms were calculated for idealised positions. 89 parameters were refined with one restraint. $R_1 = 0.037$ for 1136 reflections with $I > 2\sigma(I)$ and $wR_2 = 0.097$ for 1607 reflections, $S = 0.937$, residual electron density was between -0.26 and 0.19 e Å⁻³. Geometry calculations and checks for higher symmetry were performed with the PLATON program.^[32]

CCDC 1046565 (**1a**) contains the supplementary crystallographic data for this paper. These data are provided free of charge by The Cambridge Crystallographic Data Centre

X-ray crystal-structure determination of 2a

Crystals suitable for XRD were obtained by cooling a saturated solution of **2a** in pentane. Crystallographic data: $C_{10}H_{13}N_4P$; $M_r = 220.21$; $0.45 \times 0.09 \times 0.09$ mm³; colourless needles; monoclinic; $P2_1$; $a = 6.2161(13)$, $b = 11.251(3)$, $c = 8.1840(19)$ Å; $\alpha = 90$, $\beta = 92.885(18)$, $\gamma = 90^\circ$; $V = 571.6(2)$ Å³; $Z = 2$; $D_x = 1.280$ g cm⁻³; $\mu = 0.214$ mm⁻¹; 6489 reflections were measured by using a Stoe IPDS 2T diffractometer with a rotating anode ($Mo_{K\alpha}$ radiation; $\lambda = 0.71073$ Å) up to a resolution of $\sin \theta / \lambda_{max} = 0.69$ Å⁻¹ at a tempera-

ture of 200 K; 1796 reflections were unique ($R_{\text{int}}=0.159$). The structures were solved with SHELXS-2013^[31] by using direct methods and refined with SHELXL-2013^[31] on F^2 for all reflections. Non-hydrogen atoms were refined by using anisotropic displacement parameters. The positions of the hydrogen atoms were calculated for idealised positions. 140 parameters were refined with one restraint. $R_1=0.070$ for 1796 reflections with $I > 2\sigma(I)$ and $wR_2=0.188$ for 3082 reflections, $S=0.906$, residual electron density was between -0.50 and $0.58 \text{ e}\text{\AA}^{-3}$. Geometry calculations and checks for higher symmetry were performed with the PLATON program.^[32]

CCDC 1046566 (**2a**) contains the supplementary crystallographic data for this paper. These data are provided free of charge by The Cambridge Crystallographic Data Centre.

X-ray crystal-structure determination of 3a

Crystals suitable for XRD were obtained by cooling a saturated solution of **3a** in pentane. Crystallographic data: $\text{C}_{10}\text{H}_{13}\text{N}_4\text{P}$; $M_r=220.21$; $0.34 \times 0.09 \times 0.08 \text{ mm}^3$; colourless cylinders, monoclinic; $P2_1/m$; $a=6.8490(7)$, $b=7.0770(12)$, $c=12.248(4) \text{ \AA}$; $\alpha=90$, $\beta=106.236(13)$, $\gamma=90^\circ$; $V=570.0(2) \text{ \AA}^3$; $Z=2$; $D_x=1.283 \text{ g cm}^{-3}$; $\mu=0.215 \text{ mm}^{-1}$; 2965 reflections were measured by using a Stoe IPDS 2T diffractometer with a rotating anode ($\text{Mo}_{K\alpha}$ radiation; $\lambda=0.71073 \text{ \AA}$) up to a resolution of $\sin \theta/\lambda_{\text{max}}=0.69 \text{ \AA}^{-1}$ at a temperature of 200 K. 1684 reflections were unique ($R_{\text{int}}=0.059$). The structures were solved with SHELXS-2013^[31] by using direct methods and refined with SHELXL-2013^[31] on F^2 for all reflections. Non-hydrogen atoms were refined by using anisotropic displacement parameters. The positions of the hydrogen atoms were calculated for idealised positions. 89 parameters were refined with one restraint. $R_1=0.040$ for 1154 reflections with $I > 2\sigma(I)$ and $wR_2=0.094$ for 1627 reflections, $S=0.947$, residual electron density was between -0.25 and $0.26 \text{ e}\text{\AA}^{-3}$. Geometry calculations and checks for higher symmetry were performed with the PLATON program.^[32]

CCDC 1046564 (**3a**) contains the supplementary crystallographic data for this paper. These data are provided free of charge by The Cambridge Crystallographic Data Centre.

X-ray crystal-structure determination of 7a

Crystals suitable for XRD were obtained by cooling a hot saturated solution of **7a** in dichloromethane. Crystallographic data: $\text{C}_{13}\text{H}_{13}\text{BrN}_4\text{O}_3\text{PRE}\cdot\text{CH}_2\text{Cl}_2$; $M_r=655.28$; $0.34 \times 0.09 \times 0.08 \text{ mm}^3$; yellow needles, triclinic; $P\bar{1}$; $a=13.4120(11)$, $b=18.0785(18)$, $c=8.6707(8) \text{ \AA}$; $\alpha=89.999(8)$, $\beta=91.816(7)$, $\gamma=89.998(7)^\circ$; $V=570.0(2) \text{ \AA}^3$; $Z=4$; $D_x=2.071 \text{ g cm}^{-3}$; $\mu=8.0355 \text{ mm}^{-1}$; 22878 reflections were measured by using a Stoe IPDS 2T diffractometer with a rotating anode ($\text{Mo}_{K\alpha}$ radiation; $\lambda=0.71073 \text{ \AA}$) up to a resolution of $\sin \theta/\lambda_{\text{max}}=0.69 \text{ \AA}^{-1}$ at a temperature of 200 K. The reflections were corrected for absorption and scaled on the basis of multiple measured reflections by using the X-Red program (0.73–0.91 correction range).^[30] 11254 reflections were unique ($R_{\text{int}}=0.222$). The structures were solved with SHELXS-2013^[27] by using direct methods and refined with SHELXL-2013^[31] on F^2 for all reflections. Non-hydrogen atoms were refined by using anisotropic displacement parameters. The positions of the hydrogen atoms were calculated for idealised positions. 475 parameters were refined with one restraint. $R_1=0.054$ for 4608 reflections with $I > 2\sigma(I)$ and $wR_2=0.082$ for 11254 reflections, $S=0.774$, residual electron density was between -0.25 and $0.26 \text{ e}\text{\AA}^{-3}$. Geometry calculations and checks for higher symmetry were performed with the PLATON program.^[32]

CCDC 1046567 (**7a**) contains the supplementary crystallographic data for this paper. These data are provided free of charge by The Cambridge Crystallographic Data Centre.

X-ray crystal-structure determination of 8a

Crystals suitable for XRD were obtained by cooling a hot saturated solution of **8a** in dichloromethane. Crystallographic data: $\text{C}_{14}\text{H}_{14}\text{BrN}_4\text{O}_3\text{Re}\cdot\text{CH}_2\text{Cl}_2$; $M_r=637.33$; $0.13 \times 0.10 \times 0.08 \text{ mm}^3$; yellow rhombus; monoclinic; $P2_1/c$; $a=12.5797(10)$, $b=8.8545(5)$, $c=19.1529(15) \text{ \AA}$; $\alpha=90$, $\beta=106.558(6)$, $\gamma=90^\circ$; $V=2043.9(3) \text{ \AA}^3$; $Z=4$; $D_x=2.071 \text{ g cm}^{-3}$; $\mu=8.183 \text{ mm}^{-1}$. 15327 reflections were measured by using a Stoe IPDS 2T diffractometer with a rotating anode ($\text{Mo}_{K\alpha}$ radiation; $\lambda=0.71073 \text{ \AA}$) up to a resolution of $\sin \theta/\lambda_{\text{max}}=0.69 \text{ \AA}^{-1}$ at a temperature of 200 K. The reflections were corrected for absorption and scaled on the basis of multiple measured reflections by using the X-Red program (0.47–0.58 correction range).^[30] 5482 reflections were unique ($R_{\text{int}}=0.054$). The structures were solved with SHELXS-2013^[31] by using direct methods and refined with SHELXL-2013^[31] on F^2 for all reflections. Non-hydrogen atoms were refined by using anisotropic displacement parameters. The positions of the hydrogen atoms were calculated for idealised positions; 239 parameters were refined with one restraint. $R_1=0.034$ for 3653 reflections with $I > 2\sigma(I)$ and $wR_2=0.069$ for 5482 reflections, $S=0.986$, residual electron density was between -1.33 and $1.18 \text{ e}\text{\AA}^{-3}$. Geometry calculations and checks for higher symmetry were performed with the PLATON program.^[32]

CCDC 1046568 (**8a**) contains the supplementary crystallographic data for this paper. These data are provided free of charge by The Cambridge Crystallographic Data Centre.

Determination of optical data

UV/Vis spectra were recorded at room temperature on a Varian Cary 5000 UV/Vis/near-IR spectrophotometer. Luminescence spectra were recorded at room temperature with a FS920 Steady State Fluorimeter (M300, UC920, CD920/CD930, S900) equipped with a xenon lamp (Xe900). All spectra were recorded in CH_2Cl_2 (SDS, HPLC grade) stabilised with ethanol, with concentrations of 5.10^{-6} , 10^{-5} , 5.10^{-5} and 10^{-4} M . Quantum yields were calculated relative to quinine sulfate ($\phi=0.55$ in $0.1 \text{ N H}_2\text{SO}_4$)^[29] or to $[\text{Ru}(\text{bpy})_3]^{2+}$ in H_2O , $\phi[\text{Ru}(\text{bpy})_3]^{2+}=4.2\%$)^[29] by using Equation (1):

$$Q_x/Q_r = [A_r(\lambda)/A_x(\lambda')] [n_x^2/n_r^2] [D_x/D_r] \quad (1)$$

in which A is the absorbance at the excitation wavelength (λ), n is the refractive index and D is the integrated luminescence intensity; r and x represent reference and sample, respectively. Excitations of reference and sample compounds were performed at the maximum wavelength of the molecules.

Acknowledgements

Financial support from OTKA K 105417, Balaton PHC (830386K)–FR_12_TET_A044DF3B and COST CM10302 (SIPS) and the Bolyai Fellowship for D.S. is gratefully acknowledged. C.M. thanks the Deutsche Forschungsgemeinschaft (DFG), the European Initial Training Network SusPhos (317404) and the Free University of Berlin, Institute of Chemistry and Biochemistry, for financial support.

Keywords: coordination modes · density functional calculations · heterocycles · luminescence · phosphorus

- [1] a) C. Müller, J. A. W. Sklorz, I. de Krom, A. Loibl, M. Habicht, M. Bruce, G. Pfeifer, J. Wiecko, *Chem. Lett.* **2014**, *43*, 1390–1404; b) P. Roesch, J. Nitsch, M. Lutz, J. Wiecko, A. Steffen, C. Müller, *Inorg. Chem.* **2014**, *53*, 9855–9859; c) J. Moussa, T. Cheminel, G. R. Freeman, L.-M. Chamoreau, J. A. G. Williams, H. Amouri, *Dalton Trans.* **2014**, *43*, 8162; d) C. Müller, L. E. E. Broeckx, I. de Krom, J. J. M. Weemers, *Eur. J. Inorg. Chem.* **2013**, 187; e) C. Müller, D. Vogt, in *Catalysis and Material Science Applications* (Eds.: M. Peruzzini, L. Gonsalvi), Springer, Heidelberg, **2011**, Vol. 36, Chapter 6; f) C. Müller, in *Phosphorus Ligand Effects in Homogeneous Catalysis: Design and Synthesis* (Eds.: P. C. J. Kamer, P. W. N. M van Leeuwen), Wiley-VCH, Weinheim, **2012**; g) L. Kollár, G. Keglevich, *Chem. Rev.* **2010**, *110*, 4257; h) J. I. Bates, J. Dugal-Tessier, D. P. Gates, *Dalton Trans.* **2010**, *39*, 3151; i) B. Breit, R. Winde, T. Mackewitz, R. Paciello, K. Harms, *Chem. Eur. J.* **2001**, *7*, 3106.
- [2] a) A. Loibl, I. de Krom, E. A. Pidko, M. Weber, J. Wiecko, C. Müller, *Chem. Commun.* **2014**, *50*, 8842; b) I. de Krom, L. E. E. Broeckx, M. Lutz, C. Müller, *Chem. Eur. J.* **2013**, *19*, 3676; c) I. de Krom, E. A. Pidko, M. Lutz, C. Müller, *Chem. Eur. J.* **2013**, *19*, 7523.
- [3] a) L. Nyulászi, T. Veszprémi, J. Réffy, B. Burkhardt, M. Regitz, *J. Am. Chem. Soc.* **1992**, *114*, 9080–9084; b) L. Nyulászi, *Chem. Rev.* **2001**, *101*, 1229–1246.
- [4] a) M. Ghalib, L. Könczöl, L. Nyulászi, G. J. Palm, C. Schulzke, J. W. Heinicke, *Dalton Trans.* **2015**, *44*, 1769–1774; b) M. Ghalib, L. Könczöl, L. Nyulászi, P. G. Jones, G. J. Palm, J. W. Heinicke, *Dalton Trans.* **2014**, *43*, 51–54; c) M. Ghalib, P. G. Jones, G. J. Palm, J. W. Heinicke, *RSC Adv.* **2013**, *3*, 17726–17731; d) B. Niaz, F. Iftikhar, M. K. Kindermann, P. G. Jones, J. W. Heinicke, *Eur. J. Inorg. Chem.* **2013**, 4220–4227; e) B. R. Aluri, B. Niaz, M. K. Kindermann, P. G. Jones, J. W. Heinicke, *Dalton Trans.* **2011**, *40*, 211–224; f) M. S. S. Adam, P. G. Jones, J. W. Heinicke, *Eur. J. Inorg. Chem.* **2010**, 3307–3316; g) T. Veszprémi, L. Nyulászi, L. J. Réffy, J. W. Heinicke, *J. Phys. Chem.* **1992**, *96*, 623–626; h) L. Nyulászi, G. Csonka, J. Réffy, T. Veszprémi, J. W. Heinicke, *J. Organomet. Chem.* **1989**, *373*, 49–56.
- [5] J. A. W. Sklorz, S. Hoof, M. G. Sommer, F. Weißer, M. Weber, J. Wiecko, B. Sarkar, C. Müller, *Organometallics* **2014**, *33*, 511.
- [6] See, for example: a) J. Schneider, H. Jia, J. T. Muckerman, E. Fujita, *Chem. Soc. Rev.* **2012**, *41*, 2036–2051; b) A. J. Lees, *Photophysics of Organometallics*, in *Top. Organomet. Chem.*, Vol. 29 (Eds.: M. Beller, J. M. Brown, P. H. Dixneuf, J. Dupont, A. Fürstner, F. Glorius, L. J. Gooßen, T. Ikariya, S. Nolan, J. Okuda, L. A. Oro, Q.-L. Zhou), Springer, Heidelberg, **2010**; c) H. Takeda, O. Ishitani, *Coord. Chem. Rev.* **2010**, *254*, 346.
- [7] *Top. Heterocycl. Chem. Click Triazoles*, Vol. 28 (Eds.: B. U. W. Maes, J. Cossy, S. Polanc), Springer, Heidelberg, **2012**.
- [8] Ch. K. Lowe-Ma, R. A. Nissan, W. S. Wilson, *J. Org. Chem.* **1990**, *55*, 3755–3761.
- [9] a) W. K. C. Lo, G. S. Huff, J. R. Cubanski, A. D. W. Kennedy, C. J. McAdam, D. A. McMorran, K. C. Gordon, J. D. Crowley, *Inorg. Chem.* **2015**, *54*, 1572–1587; b) S. Jindabot, K. Teerachanan, P. Thongkam, S. Kiatisevi, T. Khamnaen, P. Phiriyawirut, S. Charoenchaidet, T. Sooksimuang, P. Kongsaeree, P. Sangtrirutnugul, *J. Organomet. Chem.* **2014**, *750*, 35–40; c) H. Bertrand, S. Clède, R. Guillot, F. Lambert, G. Policar, *Inorg. Chem.* **2014**, *53*, 6204–6223; d) T. Y. Kim, A. B. S. Elliott, K. J. Shaffer, C. J. McAdam, K. C. Gordon, J. D. Crowley, *Polyhedron* **2013**, *52*, 1391–1398; e) Q. Zhang, X. Wang, C. Cheng, R. Zhu, N. Liu, Y. Hu, *Org. Biomol. Chem.* **2012**, *10*, 2847–2854; f) P. M. Guha, H. Phan, J. S. Kinyon, W. S. Brotherton, K. Sreenath, J. T. Simmons, Z. Wang, R. J. Clark, N. S. Dalal, M. Shatruk, L. Zhu, *Inorg. Chem.* **2012**, *51*, 3465–3477; g) B. Chattopadhyay, C. I. Rivera Vera, S. Chuprakov, V. Gevorgyan, *Org. Lett.* **2010**, *12*, 2166–2169.
- [10] a) H. Chen, W. Delaunay, L. Yu, D. Joly, Z. Wang, J. Li, Z. Wang, C. Lescop, D. Tondelier, B. Geffroy, Z. Duan, M. Hissler, F. Mathey, R. Réau, *Angew. Chem. Int. Ed.* **2012**, *51*, 214–217; *Angew. Chem.* **2012**, *124*, 218–221; b) D. Joly, D. Tondelier, V. Deborde, B. Geffroy, M. Hissler, R. Réau, *New. J. Chem.* **2010**, *34*, 1603; c) H. Su, O. Fadhel, C.-J. Yang, T.-Y. Cho, C. Fave, M. Hissler, C.-C. Wu, R. Réau, *J. Am. Chem. Soc.* **2006**, *128*, 983; d) T. Baumgartner, R. Réau, *Chem. Rev.* **2006**, *106*, 4681.
- [11] a) L. Nyulászi, T. Veszprémi, T. J. Réffy, *J. Phys. Chem.* **1993**, *97*, 4011–4015; b) F. Mathey, J. F. Nixon, K. Dillon, *Phosphorus the Carbon Copy*, Wiley, Hoboken, **1998**.
- [12] G. Becker, G. Gresser, W. Uhl, *Z. Naturforsch. B* **1981**, *36*, 16.
- [13] a) S. M. Mansell, M. Green, R. J. Kilby, M. Murray, C. A. Russell, *C. R. Chim.* **2010**, *13*, 1073–1081; b) J. G. Cordaro, D. Stein, H. Rügger, H. Grützmacher, *Angew. Chem. Int. Ed.* **2006**, *45*, 6159–6162; *Angew. Chem.* **2006**, *118*, 6305–6308.
- [14] a) Y. Y. C. Yeung Lam Ko, R. Carrié, A. Muench, G. Becker, *J. Chem. Soc. Chem. Commun.* **1984**, 1634; b) Y. Y. C. Yeung Lam Ko, R. Carrié, *J. Chem. Soc. Chem. Commun.* **1984**, 1640.
- [15] a) S. L. Choong, A. Nafady, A. Stasch, A. M. Bond, C. Jones, *Dalton Trans.* **2013**, *42*, 7775–7780; b) S. L. Choong, C. Jones, A. Stasch, *Dalton Trans.* **2010**, *39*, 5774–5776.
- [16] a) Th. A. van der Knaap, Th. C. Klebach, F. Visser, F. Bickelhaupt, P. Ros, E. J. Baerends, C. H. Stam, M. Konijn, *Tetrahedron* **1984**, *40*, 765–776; b) J. J. Daly, *J. Chem. Soc. Abs.* **1964**, 3799.
- [17] N. Mézailles, F. Mathey, P. Le Floch, *Prog. Inorg. Chem.* **2001**, *49*, 455.
- [18] a) L. Nyulászi, *J. Phys. Chem.* **1996**, *100*, 6194–6198; b) L. Nyulászi, *Inorg. Chem.* **1996**, *35*, 4690–4693, c) L. Nyulászi, *Tetrahedron* **2000**, *56*, 79–84.
- [19] For pnictogen interactions, see: S. Scheiner, *Acc. Chem. Res.* **2013**, *46*, 280–288.
- [20] a) R. F. W. Bader, *Atoms in Molecules: A Quantum Theory*, Oxford University Press, Oxford, **1990**; b) R. F. W. Bader, *Acc. Chem. Res.* **1985**, *18*, 9–15.
- [21] See, for example: L. E. E. Broeckx, M. Lutz, D. Vogt, C. Müller, *Chem. Commun.* **2011**, *47*, 2003–2005.
- [22] A. Maisonia, P. Serafin, M. Traïkia, E. Debiton, V. Théry, D. J. Aitken, P. Lemoine, B. Viosat, A. Gautier, *Eur. J. Inorg. Chem.* **2008**, 298–305.
- [23] Z. Benkő, L. Nyulászi, *Top. Heterocycl. Chem.* **2009**, *19*, 27–83.
- [24] A. Modelli, B. Hajgató, J. F. Nixon, L. Nyulászi, *J. Phys. Chem. A* **2004**, *108*, 7440–7447.
- [25] Gaussian 09, Revision B.01, M. J. Frisch, G. W. Trucks, H. B. Schlegel, G. E. Scuseria, M. A. Robb, J. R. Cheeseman, G. Scalmani, V. Barone, B. Menonucci, G. A. Petersson, H. Nakatsuji, M. Caricato, X. Li, H. P. Hratchian, A. F. Izmaylov, J. Bloino, G. Zheng, J. L. Sonnenberg, M. Hada, M. Ehara, K. Toyota, R. Fukuda, J. Hasegawa, M. Ishida, T. Nakajima, Y. Honda, O. Kitao, H. Nakai, T. Vreven, J. A. Montgomery, Jr., J. E. Peralta, F. Ogliaro, M. Bearpark, J. J. Heyd, E. Brothers, K. N. Kudin, V. N. Staroverov, T. Keith, R. Kobayashi, J. Normand, K. Raghavachari, A. Rendell, J. C. Burant, S. S. Iyengar, J. Tomasi, M. Cossi, N. Rega, J. M. Millam, M. Klene, J. E. Knox, J. B. Cross, V. Bakken, C. Adamo, J. Jaramillo, R. Gomperts, R. E. Stratmann, O. Yazyev, A. J. Austin, R. Cammi, C. Pomelli, J. W. Ochterski, R. L. Martin, K. Morokuma, V. G. Zakrzewski, G. A. Voth, P. Salvador, J. J. Dannenberg, S. Dapprich, A. D. Daniels, O. Farkas, J. B. Foresman, J. V. Ortiz, J. Cioslowski, and D. J. Fox, Gaussian, Inc., Wallingford CT, **2010**.
- [26] J.-D. Chai, M. Head-Gordon, *Phys. Chem. Chem. Phys.* **2008**, *10*, 6615–6620.
- [27] G. Schaftenaar, J. H. Nordik, *J. Comput. Aided Mol. Des.* **2000**, *14*, 123–134.
- [28] J. Andersen, U. Madsen, F. Björkling, X. Liang, *Synlett* **2005**, *14*, 2209–2213.
- [29] A. M. Brouwer, *Pure Appl. Chem.* **2011**, *83*, 2213–2228.
- [30] P. Coppens, in *Crystallographic Computing* (Eds.: F. R. Ahmed, S. R. Hall, C. P. Huber), Munksgaard, Copenhagen (Denmark), **1979**, pp. 255–270.
- [31] G. M. Sheldrick, *Acta Crystallogr. Sect. A* **2008**, *64*, 112–122.
- [32] A. L. Spek, *Acta Crystallogr. Sect. D* **2009**, *65*, 148–155.

Received: March 12, 2015

Published online on June 26, 2015